HUMAN KIDNEY-DERIVED CELLS AMELIORATE ACUTE KIDNEY INJURY WITHOUT ENGRAFTING INTO RENAL TISSUE

Running title: human kidney cells improve AKI without engrafting

Ilaria Santeramo[1]*, Zeneida Herrera Perez[2]*, Ana Illera[1], Arthur Taylor[1], Simon Kenny[3], Patricia Murray[1§], Bettina Wilm[1§], Norbert Gretz[2§]

1 Centre for Preclinical Imaging, Department of Cellular and Molecular Physiology, Institute of Translational Medicine, the University of Liverpool, Liverpool, United Kingdom

2 Medical Research Center, Medical Faculty Mannheim, University of Heidelberg, Heidelberg, Germany

3 Department of Paediatric Surgery and Urology, Alder Hey Children's NHS Trust, Liverpool, United Kingdom

* Contributed equally

§ Joint senior authors

Author contributions

Ilaria Santeramo: Conception and design, Collection and/or assembly of data, Data analysis and interpretation, Manuscript writing, Final approval of manuscript

Zeneida Herrera Perez: Conception and design, Collection and/or assembly of data, Data analysis and interpretation, Final approval of manuscript

Arthur Taylor, Ana Illera: Collection and/or assembly of data, Final approval of manuscript

Simon Kenny: Provision of study material

Norbert Gretz, Patricia Murray and Bettina Wilm: Conception and design, Financial Support, Data analysis and interpretation, Manuscript writing, Final approval of manuscript

Author for correspondence:

Dr Bettina Wilm, PhD, University of Liverpool, Department of Cellular and Molecular Physiology, Crown Street, Liverpool L69 3BX, +44-151-7954988, b.wilm@liverpool.ac.uk

4-6 key words/phrases: Cisplatin-induced nephropathy in nude rats, human kidney progenitor cells, CD133, regenerative medicine therapies, transcutaneous GFR measurement

ABSTRACT

Previous studies have suggested that $CD133^+$ cells isolated from human kidney biopsies have the potential to ameliorate injury following intravenous (IV) administration in rodent models of kidney disease by integrating into damaged renal tissue and generating specialised renal cells. However, whether renal engraftment of $CD133^+$ cells is a prerequisite for ameliorating injury has not yet been unequivocally resolved. Here, we have established a cisplatin-induced nephropathy model in immunodeficient rats to assess the efficacy of $CD133^+$ human kidney cells in restoring renal health, and to determine the fate of these cells after systemic administration. Specifically, following IV administration, we evaluated the impact of the $CD133^+$ cells on renal function by undertaking longitudinal measurements of the glomerular filtration rate using a novel transcutaneous device. Using histological assays, we assessed whether the human kidney cells could promote renal regeneration, and if this was related to their ability to integrate into the damaged kidneys. Our results show that both $CD133^+$ and $CD133^-$ cells improve renal function and promote renal regeneration to a similar degree. However, this was not associated with engraftment of the cells into the kidneys. Instead, after IV administration, both cell types were exclusively located in the lungs, and had disappeared by 24 hours. Our data therefore indicate that renal repair is not mediated by $CD133^+$ cells homing to the kidneys and generating specialised renal cells. Instead, renal repair is likely to be mediated by paracrine or endocrine factors.

INTRODUCTION

Acute kidney injury (AKI) is associated with an abrupt decline in renal function, and is reported to have a mortality rate ranging from 18% to 80%[1,2]. The severity and duration of the acute injury correlates with the incidence of progression to chronic or even end stage renal disease (ESRD)[3]. Successful therapeutic interventions of AKI may not only promote recovery from acute injury, but could also decrease the incidence of ESRD.

Cisplatin is a chemotherapy drug that is used to treat a wide range of solid tumours[4], but can cause severe nephrotoxicity, which is associated with 20-40% reduction in the glomerular filtration rate (GFR), increased serum urea, elevated serum creatinine (sCr) and acute tubular necrosis[5,6].

In rodent models, cisplatin-induced AKI is routinely used to test the efficacy of novel therapies[7-11], including a range of cell-based regenerative medicine therapies[12]. Studies which tested the efficacy of mesenchymal stem/stromal cells (MSCs) showed that these cells promote repair through the secretion of paracrine factors that stimulate the regeneration of host renal tissue[12-14]. In contrast, nephron progenitor cells derived from human fetal kidneys appear to improve renal health by integrating into damaged rodent kidneys and generating specialised renal cells[15].

Recently, a population of putative progenitor cells expressing the glycosylated isoform of CD133 (Prominin-1) was identified in human adult kidneys[16,17]. CD133 is a marker of cancer stem cells and has been used to isolate stem and progenitor cells from several tissues[18]. Human adult kidney-derived $CD133^+$ cells have been shown to ameliorate injury following intravenous (IV) administration in mouse models of glycerol-induced rhabdomyolysis[16,19,20] and adriamycin-induced nephropathy[17]. Specifically, it was suggested that $CD133^+$ cells ameliorate injury by engrafting into the kidneys and differentiating into specialised renal cells[17,19]. These observations have raised the prospect of developing autologous cell therapies to replace damaged renal tissue in patients with kidney disease.

In order to track the fate of exogenous cells in preclinical models, cells are frequently labelled using membrane-bound dyes in order to allow their detection in histological sections at the study end point[17,19,21]. In previous studies assessing the role of $CD133^+$ kidney-derived cells in ameliorating renal injury, cells labelled with the lipophilic fluorescent dye, PKH26, appeared to engraft in the kidney following IV administration and express markers of podocytes and proximal tubule cells (PTCs)[17,19,21]. However, PKH26 has been shown to be an unreliable tracking agent because it can be transferred to host cells, leading to false positive results[22,23].

In this study, we aimed to accurately assess the improvement of renal function in response to $CD133^+$ human kidney cell administration in rats after cisplatin-induced AKI, and compare the therapeutic efficacy of the $CD133^+$ cells with a negative control population of $CD133^-$ cells. The GFR is the most accurate measure of renal excretory function but classical GFR measurements involve the need for repeated blood and/or continuous urine sampling over a prolonged time period (5-24h), which is difficult to obtain in rodent models. In order to monitor kidney function, we used a novel transcutaneous device to determine longitudinally the half-life ($t_{1/2}$) of fluorescein isothiocyanate (FITC)-sinistrin, a molecule that is exclusively filtered by the kidneys, as a measure of the GFR[24-27]. The device has recently been used by our group to monitor renal function in a mouse adriamycin model, where it was found to be a good predictor of histological damage[28]. In the current study, we measured FITC-sinistrin $t_{1/2}$ before cisplatin administration, before cell injection and at several points up to day 14 in rats administered with either $CD133^+$ or $CD133^-$ human kidney cells, or saline (control group), to determine for each individual animal the extent by which the cell treatment affected kidney function.

A further aim was to identify any association between therapeutic efficacy and the extent of renal engraftment. To address this question, we introduced a green fluorescent protein (GFP) reporter gene into the $CD133^+$ and $CD133^-$ cells so that their location within specific organs

could be analysed histologically. We also labelled the cells with the lipophilic dye, PKH26, to investigate whether there was any propensity for this dye to separate from the GFP^+ kidney cells and label host cells, thereby giving false positive results.

MATERIALS AND METHODS

Isolation and lentiviral transduction of human kidney cells.

Infant renal tissue was obtained from kidneys deemed unsuitable for transplantation via UK National Health Service Blood and Transfusion (NHSBT). The tissue was minced in small pieces in sterile conditions and digested with collagenase I (1mg/mL, C0130, Sigma) for 90 minutes at 37˚C, centrifuged and incubated with DMEM/F12 containing DNAse I (1%) (Sigma) for 15 minutes at room temperature. The cell suspension was filtered through a 70 µm and a 40 µm sterile sieve and plated in the human renal progenitor cell (HRPC) medium previously used for fetal progenitor cells[29]. The medium was changed every two days until the cells reached 90% confluence.

Lentiviral particles were produced as previously described[30] using an unmodified eGFP vector (pHIV-eGFP, Addgene, 21373) with a multiplicity of infection (MOI) of 5, yielding >90% labelling efficiency. Typically, $2x10^5$ cells were plated 8 hours before transduction. Once attached, the cells were incubated for 16 hours in complete medium containing the appropriate amount of lentiviral particles containing 8 µg/ml of Polybrene (Sigma, H9268). The medium was then appropriately discarded, and the cells were grown in normal medium. Details regarding cell sorting, cell characterisation and immunofluorescence protocols are provided in the online methods section.

Animals

All *in vivo* experiments were conducted at the University of Heidelberg in accordance with the German Animal Protection Law and approved by the local authority

(Regierungspräsidium Nordbaden, Karlsruhe, Germany, in agreement with EU directive 2010/63/EU). 8-9 weeks old male immunodeficient athymic nude rats (Crl:NIH-Foxn1^{rnu}, Charles River Laboratories) were housed in pairs in individually ventilated cages and acclimated for 1 week before the start of the experiments.

Cisplatin-induced kidney injury

Freshly prepared cisplatin solution (Sigma, dissolved in sterile 0.9% saline (AlleMan Pharma) was administered intraperitoneally (IP) at 7mg/100g body weight. For the two-week experiment, a total of twenty male immunodeficient athymic nude rats were used. Onset of renal damage following cisplatin administration was confirmed at day 2 via measurements of FITC-sinistrin (Fresenius Kabi, Linz, Austria) $t_{1/2}$ as described below.

Renal biomarker analysis

Serum was collected from whole blood samples before the induction of damage, and then on days 7 and 14 after cisplatin administration via the ophthalmic venous plexus (orbital sinus), and stored at -20°C until use. For urine collection, the animals were housed for 16 hours in individual metabolic cages with free access to water and food. At the end of each collection period, the urine volume was recorded, and the samples were centrifuged (78g, 5 minutes) and immediately frozen at -20°C until analysed. Serum creatinine (sCr), serum urea and urine creatinine were determined using the Cobas c311 analyzer (Roche Diagnostics GmbH, Mannheim, Germany). Albumin levels in urine were determined by ELISA and the values were normalized to the amount of urinary creatinine over a 24 hour period. Assessment of glomerular filtration at baseline and on days 2, 7 and 14 after cisplatin administration was performed by administering FITC-sinistrin into the tail vein, and detecting the fluorescence signal transcutaneously for 90 minutes using a miniaturized device (Mannheim Pharma and Diagnostic, Mannheim, Germany). The FITC-sinistrin $t_{1/2}$ was computed using a specifically designed software[31].

Cell administration

Before each injection, GFP-expressing $CD133^+$ and $CD133^-$ cell populations were incubated with PKH26 (Sigma), following manufacturer's instructions. Animals that displayed renal injury by day 2 following cisplatin administration (as indicated by the FITC-sinistrin $t_{1/2}$ measurements) were randomly assigned to three groups, two of which received either 10^6 GFP-expressing $CD133^+$ or $CD133^-$ cells in a 500 µl volume of sterile phosphate-buffered saline (PBS) via lateral tail vein injection; the cisplatin-injured control group received PBS ($CD133^+$ group, 6 animals; $CD133^-$ group, 6 animals; cisplatin-injured control group, 7 animals). A scheme of the experimental design is shown in **Fig. 2A**). On day 7, cell-treated animals received a second dose of either 10^6 GFP-expressing $CD133^+$ or $CD133^-$ cells into the tail vein.

For the biodistribution study, a total of eight male immunodeficient athymic nude rats were used. After assessment of cisplatin-induced renal damage on day 2, 10^6 $CD133^+$ cells were injected into the lateral tail vein of 6 animals. 2 animals each were sacrificed at 1, 6 and 24 hours after cell injection. Additionally, 2 uninjured control animals were sacrificed 1 hour after injection of saline.

Morphological and histological analysis

For the morphological and histological analysis, 4 uninjured rats were included in the study. Immediately after culling, kidneys and lungs were excised, fixed in 4% paraformaldehyde for 24 hours and paraffin embedded or frozen for immunohistological analysis (see below). 3µm-thick paraffin sections were stained with hematoxylin and eosin (H&E) or Masson's Trichrome (MT). For the measurement of mean luminal area, 10 random fields of the renal cortex of each animal were imaged using a 20X objective. The images were transformed into black and white (B&W, 8 bit), and a B&W threshold was applied using Fiji software. The luminal areas on the edge of the image were excluded from the analysis. For measurement of

the fibrotic areas in MT-stained sections, 10 random fields of the renal cortex of each animal were imaged using a 20X objective. A colour threshold (blue) to all images was applied using Fiji software and the blue area was computed. Also, 5 to 7 MT images of two animals per group were stitched together using the 'grid-collection stitching' plug-in of the Fiji software.

Immunostaining of tissue sections

Frozen sections were blocked with 0.1% Triton-X 100 (Sigma) and 10% goat serum (Sigma) in PBS and incubated with anti-Calbindin (1:500, Sigma, C9848), anti-CD68 (1:500, Abcam, ab31630) anti-GFP (1:5000, Abcam, ab6556), anti-HLA (1:50, Santa Cruz, sc-25619), anti-human nuclei (1:200, Millipore, MAB 1281), anti-IL10 (1:200, Abcam, ab9969), anti-megalin (1:200, Acris antibodies, DM3613P) followed by incubation with the secondary antibodies Alexa Fluor® 488-coupled goat anti-rabbit IgG, Alexa Fluor® 633-coupled goat anti-mouse $IgG_{1,}$ Alexa Fluor® 647-coupled goat anti-rabbit, Alexa Fluor® 594-coupled goat anti-mouse IgG_1 (Thermo-Fisher Scientific). Nuclei were counterstained with DAPI (Invitrogen). Fluorescence images were taken using a spinning disk confocal microscope CSU-X1 (3i Marianas), coupled with a digital camera (CMOS, Hamamatsu). The megalin stitched images were composed using the 'pairwise stitching' plug-in of the Fiji software [32].

Statistics

All data are presented as mean ± standard error mean (SEM). All statistical analysis was performed using GraphPad software, and a one-way ANOVA was used to compare three or more groups. The statistical significance was assumed for a p-value (p) ≤ 0.05.

RESULTS

Human kidney-derived cells express CD133 in culture

In order to analyse the role of human kidney-derived cells in renal regeneration or repair, we generated primary cultures of renal cells by dissociating cortical fragments isolated from healthy infant renal tissue. We analysed histological sections and primary renal cell cultures for expression of CD133, which has been previously described as a marker for kidney progenitor cells[16,21,33]. Immunohistological analysis of the kidney sections demonstrated CD133 localisation in cells of the Bowman's capsule, and on the apical surface of scattered tubular cells **(Fig. 1 A)**, similar to the pattern observed in adult human kidneys[17,19,34]. Following tissue dissociation, more than 65% of the cells in the primary cultures expressed CD133, as shown by immunofluorescence (**Fig. 1 B**) and flow cytometric analysis **(Fig. 1 C)**. Since $CD133^+$ renal progenitor cells have been reported to co-express CD24[35], we verified by flow cytometry that all $CD133^+$ expressed CD24; however, only 70% of $CD24^+$ cells expressed CD133 **(Fig. 1 D)**. Thus, our results show that following isolation, the majority of the kidney-derived cells expressed CD133 in culture.

$CD133^+$ and $CD133^-$ human kidney cells ameliorate renal function

We induced kidney injury in 8-9 week old male athymic nude rats by injecting cisplatin at 7mg /100g body weight. Animals were monitored for renal function by measuring the FITC-sinistrin $t_{1/2}$ at days 2, 7 and 14, and the serum injury markers sCr and urea at days 7 and 14. In 62.5% (20 out of 32) of the rats, an increase in the FITC-sinistrin $t_{1/2}$ was detected at day 2 when compared to baseline measurements before cisplatin administration. Only these animals were used for the subsequent study by assigning them to three groups which received on days 2 and 7 by IV injection either (i) $CD133^+$ passage 5 (P5) cells, (ii) $CD133^-$ P5 cells, or (iii) saline (**Fig. 2A).**

Prior to injection, the cells had been transduced with a pHIV-eGFP vector and sorted for CD133 expression using FACS **(Supplemental Fig. 1A-D)**. Flow cytometry demonstrated that at passage 5, the GFP^+ $CD133^+$ population had a purity of 91.36 ± 9.17 %, and the GFP^+ $CD133^-$ population had a purity of 92.99 ± 6.00 % (n=3) **(Fig. 2B)**. The cell morphologies of the two populations after GFP-lentivirus transduction were very similar to the un-transduced $CD133^+$ and $CD133^-$ cells **(Supplemental Fig. 1 E)**. The $CD133^+$ population appeared epithelial-like, whereas the $CD133^-$ population was composed of elongated mesenchymal-like cells. Compared with $CD133^+$ cells, the $CD133^-$ cells expressed noticeably lower levels of the epithelial marker, Epcam **(Supplemental Figure 2)**. To investigate if the $CD133^-$ cells resembled MSCs, which are known to reside in the kidney[36], we performed flow cytometric analysis to determine the expression levels of key MSC markers. We found that in comparison with human bone marrow-derived MSCs, both the $CC133^+$ and $CD133^-$ cells expressed very low levels of the MSC markers, CD90 and CD105 **(Supplemental Figure 2)**. Thus, given that the $CD133^-$ cells are non-epithelial, and are also not MSCs, it is most likely that they are renal interstitial cells, which include various cell types, including interstitial fibroblasts[37]. Prior to administering the cells, as an additional method to track them, the cells were labelled with the lipophilic fluorescent dye, PKH26, which had been used in previous studies[17,19,21,38,39].

Sequential measurements of the FITC-sinistrin $t_{1/2}$ clearance revealed that on day 7, the FITC-sinistrin $t_{1/2}$ was significantly reduced in animals that received either $CD133^+$ or $CD133^-$ cells, when compared to those of the cisplatin-injured group, indicating an improvement in renal function **(Fig 2C, Supplemental Table 1)**. It is important to note that no significant differences in FITC-sinistrin $t_{1/2}$ were observed between animals of the two cell-treated groups. By day 14, the FITC-sinistrin $t_{1/2}$ had decreased in the cisplatin-injured animals, and was no longer significantly different from that of the cell-treated groups. No further decrease

in the FITC-sinistrin $t_{1/2}$ was observed in the cell-treated groups after day 7, indicating that the second cell injection had no additional beneficial effects on renal function **(Fig. 2C)**.

In addition to the improvement in glomerular filtration function, the administration of $CD133^+$ cells resulted in statistically reduced sCr (by 72.3%) and urea (by 74.2%) at day 7. In the $CD133^-$-treated group, sCr and urea values were also lower than in rats from the cisplatin-injured group, though these were not statistically significant **(Fig. 2D-E; Supplemental Table 1).** By comparing the FITC-sinistrin $t_{1/2}$ values at day 14 with the baseline values, it could be seen that renal function was not completely restored in either the $CD133^+$ or $CD133^-$ treated rats **(Fig. 2C)**. The comparison between serum creatinine baseline and d14 values also suggested that cell treatments failed to restore levels back to baseline **(Fig. 2D)**, while the serum urea values suggested there was a complete restoration **(Fig. 2E)**. However, given that both these biomarkers are less accurate indicators of renal function than FITC-sinistrin $t_{1/2}$, we conclude that the cell therapy does not fully restore renal function.

To further investigate the degree of tubular injury at the study end-point (day 14), kidney sections were stained for the PTC marker, megalin, and the collecting tubule marker, calbindin. No differences in the pattern of calbindin staining was observed between any of the groups, but megalin staining was atypical in the cisplatin-injured rats, consistent with PTC injury **(Supplemental Figure 3 A-B)**. It is known that megalin plays an important role in re-absorbing filtered albumin[40]. Thus, to investigate if the injured rats displayed higher levels of albuminuria compared with those that received cell therapy, the urinary albumin:creatine ratio was measured at days 2, 7 and 14. The results showed that the albumin:creatinine ratio increased from day 7 to day 14 in the injured rats, but was not significantly greater than background levels in rats that received the cell therapy **(Supplemental Figure 3 C)**.

Thus, our results demonstrate that $CD133^+$ cells could ameliorate the acute phase of cisplatin-induced renal injury in nude rats when compared to cisplatin-injured animals, as shown by the significant reduction in FITC-sinistrin $t_{1/2}$, sCr, serum urea and urinary albumin **(Fig. 2C**-E

and **Supplemental Figure 3C**). Of note, $CD133^-$ cells had a similar beneficial effect on kidney function, since the differences in measurements of all 4 parameters between the $CD133^+$ and $CD133^-$ -treated animals were not significant.

$CD133^+$ and $CD133^-$ human kidney cells ameliorate histological damage

Next, we used histopathological analysis to investigate the impact of the administered cells on renal tissue health at day 14. In H&E-stained sections from kidneys of the cisplatin-injured group, abnormalities typical of acute tubular injury were observed, including cells with pyknotic nuclei and dilated tubules with flattened epithelia **(Fig. 3A)**. By contrast, these features were rarely observed in kidneys from the cell-treated groups and uninjured control kidneys **(Fig. 3A)**.

We assessed the tubular damage by measuring the mean luminal area, which revealed that the tubular luminal area of cisplatin-injured rats was significantly greater than that of the cell-treated groups and uninjured control rats (cisplatin-only: $5400\mu m^2 \pm 739$, n=7; $CD133^+$: $3000\mu m^2 \pm 218$ ($p<0.01$), n=7; $CD133^-$: $3100\mu m^2 \pm 301$ ($p<0.05$), n=6; uninjured: $1350\ \mu m \pm 26$ ($p<0.001$)) (**Fig. 3B**).

Previous studies have shown that by 14 days following cisplatin administration, extensive fibrosis is present in rat kidneys [41]. To determine whether administration of the $CD133^+$ and $CD133^-$ cells could ameliorate renal fibrosis, we performed Masson's trichrome analysis. Despite widespread tubular dilation in the cisplatin-injured group, fibrotic lesions were minimal and no significant differences were observed between the cisplatin-injured and cell-treated groups at day 14 **(Fig. 3C, D, Supplemental Fig. 4)**. The negligible degree of renal fibrosis in these animals is likely due to the fact that they lack T cells, which are known to play a key role in the development of renal fibrosis[42].

CD133$^+$ and CD133$^-$ cells do not engraft in the kidneys following intravenous administration

Previous studies have suggested that intravenously administered CD133$^+$ human kidney cells ameliorate injury by engrafting in the kidney and generating podocytes and proximal tubule cells[17,19]. MSCs, on the other hand, become entrapped in the lung following intravenous administration and ameliorate renal injury via paracrine or endocrine factors[12,14,43]. To investigate whether CD133$^+$ and CD133$^-$ human kidney cells were present in the kidneys or lungs following IV administration in the rat cisplatin model, tissue sections were analysed for the presence of GFP and PKH26 at day 14.

PKH26 could be detected in the kidneys of rats that received human kidney cells, and was typically located close to tubular or interstitial cells, but there was no evidence of any GFP$^+$ cells **(Fig. 4B-C)**. Similarly, no GFP$^+$ cells, but traces of PKH26 dye, were identified in the lungs of animals treated with human kidney cells **(Fig. 4E-F)**. As expected, neither PKH26 nor GFP$^+$ cells were found in kidneys or lungs of cisplatin-injured animals that did not receive cells **(Fig. 4A, D**, see **Supplemental Fig. 5** for a comparison between a GFP$^+$ cell and an autofluorescent cell). The presence of PKH26 in the absence of GFP suggested that PKH26 staining at day 14 was due to false positive staining of host cells. Overall, these results indicated that the administered cells were not detectable in kidneys or lungs by day 14.

To demonstrate the presence of the human kidney cells and investigate their fate at earlier time points, CD133$^+$ human kidney cells were IV injected into cisplatin-injured rats and tissue sections analysed for the presence of cells at 1, 6 and 24 hours after cell administration. Using GFP- and human-specific antibodies (i.e., against HLA and a human nuclear antigen), we could detect GFP$^+$ human cells in sections of lungs collected one hour after cell administration **(Fig. 5A-B)**. However, the presence of pyknotic nuclei and blebbing in some of the GFP$^+$ cells suggested that they were undergoing cell death. In addition, we could identify a punctate pattern of PKH26 dye in or around the cells. In sections of lungs collected

six hours after cell administration, we found both fragmented and intact GFP^+ cells. Importantly, we detected the PKH26 label not only in GFP^+ cells, but also in neighbouring GFP^- cells **(Fig. 5C-C')**. At the 24-hour time point, we could only identify the GFP signal in cell fragments close to $PKH26^+$ puncta, but not in intact cells **(Fig. 5D)**. By contrast, analysis of kidney sections at all three time points revealed only punctate PKH26 staining, but no GFP^+ cells or fragments. HLA staining was occasionally detected in the kidney, but no human nuclei were observed, confirming the lack of engraftment of intact cells in this organ **(Fig. 5E-H)**. To investigate whether the cells had engrafted in the spleen and liver, tissue sections from these organs were stained for GFP and the human-specific antigens, but only background autofluorescence could be detected (see **Supplemental Figure 6** for spleen data; liver data not shown). Therefore, our data demonstrate that following tail vein injection, the human kidney cells became entrapped in the lungs and died within 24 hours of administration. Importantly, our results provide no evidence of the cells engrafting in the kidneys.

Intravenous injection of human kidney cells leads to macrophage infiltration in the lungs

Dying cells and their fragments are known to be phagocytosed by resident macrophages[44] and dendritic cells[45]. Furthermore, the process of macrophage-based removal of apoptotic cells has been shown to inhibit inflammation via anti-inflammatory cytokines[46,47]. To determine whether macrophages were recruited to the dying human cells, we performed immunofluorescence staining for the pan-macrophage marker CD68 on sections from lungs at 1, 6 and 24 hours after administration of human kidney cells. We found that the $CD68^+$ cells were evenly distributed across the tissue in sections of control lungs from all time points **(Fig. 6A)**. By contrast, at one and six hours after cell administration, $CD68^+$ cells appeared to cluster closely around intact GFP^+ cells and GFP^+ cell fragments **(Fig. 6B, B', C)**. Confocal imaging and volume rendering of z-stacks revealed that some of the $CD68^+$ cells also contained the PKH26 label (see **Supplemental Video 1 and 2)**, suggesting that the

macrophages might be involved in phagocytosing the GFP^+ $CD133^+$ cell fragments. In sections of lungs at 24 hours after cell administration, the $CD68^+$ cells remained in clusters around small GFP-labelled fragments while intact human cells were no longer present **(Fig. 6 D, D')**. Analysis of expression of the anti-inflammatory cytokine IL10 in the lungs at 24 hours showed IL10 within and surrounding $CD68^+$ cells in close proximity to the dying human cells. These results suggest that IL10 may have been released by the macrophages following phagocytosis of the human cells (**Supplemental Figure 7**).

DISCUSSION

In this study we have shown that $CD133^+$ cells isolated from human infant renal tissue could improve renal function and ameliorate tissue damage following intravenous administration in a rat cisplatin model. These findings are consistent with previous studies that showed adult kidney-derived $CD133^+$ cells had beneficial effects following tail vein injection in mouse models of glomerular and tubular injury[19,48]. However, whereas these earlier studies reported no beneficial effects of $CD133^-$ cells, we found that in the rat cisplatin model, $CD133^+$ and $CD133^-$ cells were similarly therapeutic **(Table 1)**.

CD133 has previously been identified as a marker for various types of stem cells[18], and has been reported to be a progenitor cell marker in human fetal[49] and adult kidneys[16,17,19]. In the fetal kidney, this was mainly based on evidence that CD133 was expressed in the metanephric mesenchyme[49], a population of cells within the developing mammalian kidney that gives rise to all cell types of the nephron. However, more recent analysis has shown that CD133 is not co-expressed with the bona fide nephron progenitor marker, SIX2, and is instead expressed in differentiating cells[50], suggesting that CD133 is not a progenitor marker in the fetal kidney. In adult human kidneys, CD133 is expressed in parietal epithelial cells[17] and in a small population of scattered tubular epithelial cells within the proximal and distal tubules[17,51,52], which is consistent with the staining pattern observed in infant kidneys in the current study.

The most compelling evidence for CD133 being a renal progenitor marker is based on studies showing that following IV administration into mice with renal injury, adult human kidney-derived $CD133^+$ cells could engraft in the kidneys and generate podocyte and proximal tubule cells[17,19]. However, this contrasts with our current study, where we found that following tail vein injection, infant kidney-derived $CD133^+$ and $CD133^-$ cells did not engraft into injured kidneys, and instead, were entrapped in the lungs and did not survive beyond 24 hours.

A possible explanation for these apparent differences in $CD133^+$ biodistribution could be due to the fact that in the earlier studies, $CD133^+$ cells were isolated from the 'normal' regions of adult kidneys affected by tumours. This raises the possibility that the adult $CD133^+$ cells might have been renal carcinoma cells that had migrated from the primary lesion into the surrounding normal tissue, and perhaps as a result of their malignant phenotype, were able to traverse the pulmonary capillaries. It must also be considered that in the earlier studies, the cells were used at passage 0 (P0), whereas in the current study, the cells were used at passage 5 (P5). Therefore, we cannot discount the possibility that P0 cells might be able to pass through the lung, whereas P5 cells cannot. However, it is more likely that the high level of renal engraftment reported in these previous studies was due to a combination of autofluorescence[53] and false-positive staining, for it is known that the lipophilic dye, PKH26, that was used to monitor the fate of the $CD133^+$ cells, can readily transfer to host cells[22,54]. Indeed, the problem with PKH26 false-positive staining was demonstrated in the current study, where we detected PKH26 dye in the kidneys despite the GFP-labelled $CD133^+$ cells being located solely in the lungs. It is also worth noting that the high levels of renal engraftment reported in some earlier studies would be difficult to achieve (see **Supplemental Table 2**)[17].

The lack of renal engraftment in the current study indicates that the therapeutic effects of the $CD133^+$ and $CD133^-$ cells in the rat cisplatin model are mediated by paracrine or endocrine factors. Our results are similar to those of a previous study by Geng and colleagues[14]

investigating the therapeutic effects of MSCs in a mouse tubular injury model, where it was found that following tail vein administration, cells were mainly located in the lungs and were not detected in the kidneys. Further experiments showed that the MSCs ameliorated renal injury by increasing the number of alternatively-activated (M2) macrophages[14]. It is well-established that MSCs have immunomodulatory effects and ameliorate renal injury by paracrine mechanisms[12,13], but more recently, it has been shown that the therapeutic effects of various other cell types, including human induced pluripotent stem cell (iPSC)-derived nephron progenitors, are also mediated by paracrine factors[55]. For instance, Toyohara and co-workers showed that if iPSC-derived nephron progenitors were injected into the renal parenchyma of mice with ischemia reperfusion injury, the cells could integrate and generate new tubular cells, but did not ameliorate injury[55]. On the other hand, if the cells were injected under the kidney capsule, they did not integrate into the kidney, but had a significant therapeutic effect. Likewise, the administration of rat kidney-derived renal tubule cells into rats with subtotal nephrectomy reduced leucocyte infiltration and inflammation, and promoted repair via paracrine mechanisms[56]. Similar findings have been reported for other organs, such as the liver and heart, where it was respectively shown that the therapeutic effects of embryonic stem cell-derived hepatocytes and cardiac stem cells were mediated by trophic factors[57,58].

Our observation that the $CD133^+$ and $CD133^-$ cells had similar therapeutic effects in the rat cisplatin model is interesting, especially given the differences in phenotype between the two cell types, with the former being predominantly epithelial cells, and the latter having a more mesenchymal-like morphology. An important finding from our study was that similarly to MSCs[59], the human kidney cells died quite rapidly in the lung following intravenous administration and induced the infiltrating macrophages to express IL10. It is well established that apoptotic cells release 'find me' signals, such as fractalkine and lysophosphatidylcholine, which serve as chemo-attractants for macrophages[45]. Moreover, following the phagocytosis of

apoptotic cell debris, macrophages become polarised towards an alternatively activated (M2) phenotype and secrete anti-inflammatory cytokines, such as IL10[60], which has been shown to ameliorate cisplatin-induced renal injury in rodents[61]. Thus, it is possible that the therapeutic effects of the dying human kidney cells might have been due to their ability to trigger macrophages to secrete IL10 (and perhaps other anti-inflammatory cytokines), which could stimulate renal repair by promoting an early resolution of the inflammatory response. In support of a role for dying cells, Thum and colleagues[46] have previously hypothesised that immunomodulatory effects can be triggered by the apoptosis of exogenous stem cells, and more recently, Luk et al have shown that heat-inactivated (i.e., non-viable) MSCs can modulate macrophages and induce a dramatic increase in IL10 expression in mice[62]. Furthermore, dying (apoptotic) cells have also been reported to release microvesicles or apoptotic bodies which could potentially have immunomodulatory roles in kidney regeneration[63]. This is supported by the observation that microvesicles isolated from MSCs have renoprotective roles in mouse models of AKI[64-66].

Though beyond the scope of the present study, by understanding the mechanisms whereby dying cells modulate the behaviour of key immune effector cells and ameliorate renal injury, it should be possible to develop safer and more effective cell-free regenerative medicine therapies in the future.

CONCLUSION

Here we present data showing that cells isolated from human infant kidneys have the potential to ameliorate functional and histological damage in rats with cisplatin-induced kidney injury. Our results demonstrate that CD133 expression in the cells is not required for their beneficial effects. Furthermore, since the human kidney cells die in the lungs shortly after their administration and are not detected in the kidneys, our findings indicate that the cells exert

their therapeutic effects via paracrine factors, and that renal engraftment is not a prerequisite for ameliorating renal injury.

Acknowledgements:

We acknowledge funding for this project from the FP7 Marie Curie Initial Training Network 'NephroTools', from the Alder Hey Children Kidney Fund and from the UKRMP hub grant 'Safety and efficacy, focussing on imaging technologies' (grant MR/K026739/1). We would like to thank Angela Platt-Higgins (University of Liverpool) for her assistance in the preparation of paraffin-embedded samples and histological stainings.

DISCLOSURE OF POTENTIAL CONFLICTS OF INTEREST

The authors indicate no potential conflicts of interest.

REFERENCES

1. Chawla LS, Kimmel PL. Acute kidney injury and chronic kidney disease: an integrated clinical syndrome. *Kidney international.* 2012;82(5):516-524.
2. Singbartl K, Kellum JA. AKI in the ICU: definition, epidemiology, risk stratification, and outcomes. *Kidney international.* 2012;81(9):819-825.
3. Chawla LS, Amdur RL, Amodeo S, Kimmel PL, Palant CE. The severity of acute kidney injury predicts progression to chronic kidney disease. *Kidney international.* 2011;79(12):1361-1369.
4. Hanigan MH, Devarajan P. Cisplatin nephrotoxicity: molecular mechanisms. *Cancer therapy.* 2003;1:47-61.
5. Miller RP, Tadagavadi RK, Ramesh G, Reeves WB. Mechanisms of Cisplatin nephrotoxicity. *Toxins.* 2010;2(11):2490-2518.
6. Ozkok A, Edelstein CL. Pathophysiology of cisplatin-induced acute kidney injury. *Biomed Res Int.* 2014;2014:967826.
7. Singh AP, Junemann A, Muthuraman A, et al. Animal models of acute renal failure. *Pharmacol Rep.* 2012;64(1):31-44.
8. Heyman SNKMRSRC. In vivo models of acute kidney injury. *Drug Discovery Today: Disease Models.* 2010;7(1-2):51-56.
9. Li J, Gui Y, Ren J, et al. Metformin Protects Against Cisplatin-Induced Tubular Cell Apoptosis and Acute Kidney Injury via AMPKalpha-regulated Autophagy Induction. *Sci Rep.* 2016;6:23975.
10. Bruno S, Grange C, Deregibus MC, et al. Mesenchymal stem cell-derived microvesicles protect against acute tubular injury. *Journal of the American Society of Nephrology : JASN.* 2009;20(5):1053-1067.
11. Yao W, Hu Q, Ma Y, et al. Human adipose-derived mesenchymal stem cells repair cisplatin-induced acute kidney injury through antiapoptotic pathways. *Exp Ther Med.* 2015;10(2):468-476.
12. Bi B, Schmitt R, Israilova M, Nishio H, Cantley LG. Stromal cells protect against acute tubular injury via an endocrine effect. *Journal of the American Society of Nephrology : JASN.* 2007;18(9):2486-2496.
13. Donizetti-Oliveira C, Semedo P, Burgos-Silva M, et al. Adipose tissue-derived stem cell treatment prevents renal disease progression. *Cell Transplant.* 2012;21(8):1727-1741.
14. Geng Y, Zhang L, Fu B, et al. Mesenchymal stem cells ameliorate rhabdomyolysis-induced acute kidney injury via the activation of M2 macrophages. *Stem cell research & therapy.* 2014;5(3):80.
15. Harari-Steinberg O, Metsuyanim S, Omer D, et al. Identification of human nephron progenitors capable of generation of kidney structures and functional repair of chronic renal disease. *EMBO Mol Med.* 2013;5(10):1556-1568.
16. Bussolati B, Bruno S, Grange C, et al. Isolation of renal progenitor cells from adult human kidney. *The American journal of pathology.* 2005;166(2):545-555.
17. Ronconi E, Sagrinati C, Angelotti ML, et al. Regeneration of glomerular podocytes by human renal progenitors. *Journal of the American Society of Nephrology : JASN.* 2009;20(2):322-332.
18. Fargeas CA. Prominin-1 (CD133): from progenitor cells to human diseases. *Future Lipidol.* 2006;1(2):213-225.
19. Angelotti ML, Ronconi E, Ballerini L, et al. Characterization of renal progenitors committed toward tubular lineage and their regenerative potential in renal tubular injury. *Stem cells.* 2012;30(8):1714-1725.
20. Grange C, Moggio A, Tapparo M, Porta S, Camussi G, Bussolati B. Protective effect and localization by optical imaging of human renal CD133+ progenitor cells in an acute kidney injury model. *Physiol Rep.* 2014;2(5):e12009.
21. Sagrinati C, Netti GS, Mazzinghi B, et al. Isolation and characterization of multipotent progenitor cells from the Bowman's capsule of adult human kidneys. *Journal of the American Society of Nephrology : JASN.* 2006;17(9):2443-2456.

22. Lassailly F, Griessinger E, Bonnet D. "Microenvironmental contaminations" induced by fluorescent lipophilic dyes used for noninvasive in vitro and in vivo cell tracking. *Blood.* 2010;115(26):5347-5354.
23. Progatzky F, Dallman MJ, Lo Celso C. From seeing to believing: labelling strategies for in vivo cell-tracking experiments. *Interface Focus.* 2013;3(3):20130001.
24. Pill J, Kraenzlin B, Jander J, et al. Fluorescein-labeled sinistrin as marker of glomerular filtration rate. *Eur J Med Chem.* 2005;40(10):1056-1061.
25. Pill J, Issaeva O, Woderer S, et al. Pharmacological profile and toxicity of fluorescein-labelled sinistrin, a novel marker for GFR measurements. *Naunyn Schmiedebergs Arch Pharmacol.* 2006;373(3):204-211.
26. Schock-Kusch D, Xie Q, Shulhevich Y, et al. Transcutaneous assessment of renal function in conscious rats with a device for measuring FITC-sinistrin disappearance curves. *Kidney international.* 2011;79(11):1254-1258.
27. Schock-Kusch D, Sadick M, Henninger N, et al. Transcutaneous measurement of glomerular filtration rate using FITC-sinistrin in rats. *Nephrology, dialysis, transplantation : official publication of the European Dialysis and Transplant Association - European Renal Association.* 2009;24(10):2997-3001.
28. Scarfe L, Rak-Raszewska A, Geraci S, et al. Measures of kidney function by minimally invasive techniques correlate with histological glomerular damage in SCID mice with adriamycin-induced nephropathy. *Sci Rep.* 2015;5:13601.
29. Price KL, Long DA, Jina N, et al. Microarray interrogation of human metanephric mesenchymal cells highlights potentially important molecules in vivo. *Physiological genomics.* 2007;28(2):193-202.
30. Pereira SM, Moss D, Williams SR, Murray P, Taylor A. Overexpression of the MRI Reporter Genes Ferritin and Transferrin Receptor Affect Iron Homeostasis and Produce Limited Contrast in Mesenchymal Stem Cells. *Int J Mol Sci.* 2015;16(7):15481-15496.
31. Herrera Perez Z, Weinfurter S, Gretz N. Transcutaneous Assessment of Renal Function in Conscious Rodents. *J Vis Exp.* 2016(109).
32. Preibisch S, Saalfeld S, Tomancak P. Globally optimal stitching of tiled 3D microscopic image acquisitions. *Bioinformatics.* 2009;25(11):1463-1465.
33. Ronconi E, Mazzinghi B, Sagrinati C, et al. [The role of podocyte damage in the pathogenesis of glomerulosclerosis and possible repair mechanisms]. *Giornale italiano di nefrologia : organo ufficiale della Societa italiana di nefrologia.* 2009;26(6):660-669.
34. Hansson J, Hultenby K, Cramnert C, et al. Evidence for a morphologically distinct and functionally robust cell type in the proximal tubules of human kidney. *Hum Pathol.* 2014;45(2):382-393.
35. Romagnani P, Remuzzi G. CD133+ renal stem cells always co-express CD24 in adult human kidney tissue. *Stem cell research.* 2014;12(3):828-829.
36. Huang Y, Chen P, Zhang CB, et al. Kidney-derived mesenchymal stromal cells modulate dendritic cell function to suppress alloimmune responses and delay allograft rejection. *Transplantation.* 2010;90(12):1307-1311.
37. Zeisberg M, Kalluri R. Physiology of the Renal Interstitium. *Clinical journal of the American Society of Nephrology : CJASN.* 2015;10(10):1831-1840.
38. Gupta AK, Jadhav SH, Tripathy NK, Nityanand S. Fetal kidney stem cells ameliorate cisplatin induced acute renal failure and promote renal angiogenesis. *World J Stem Cells.* 2015;7(4):776-788.
39. Qi S, Wu D. Bone marrow-derived mesenchymal stem cells protect against cisplatin-induced acute kidney injury in rats by inhibiting cell apoptosis. *Int J Mol Med.* 2013;32(6):1262-1272.
40. Dickson LE, Wagner MC, Sandoval RM, Molitoris BA. The proximal tubule and albuminuria: really! *Journal of the American Society of Nephrology : JASN.* 2014;25(3):443-453.
41. Kawai Y, Satoh T, Hibi D, et al. The effect of antioxidant on development of fibrosis by cisplatin in rats. *J Pharmacol Sci.* 2009;111(4):433-439.
42. Tapmeier TT, Fearn A, Brown K, et al. Pivotal role of CD4+ T cells in renal fibrosis following ureteric obstruction. *Kidney international.* 2010;78(4):351-362.

43. Sharkey J, Scarfe L, Santeramo I, et al. Imaging technologies for monitoring the safety, efficacy and mechanisms of action of cell-based regenerative medicine therapies in models of kidney disease. *Eur J Pharmacol.* 2016.
44. Fadok VA, Voelker DR, Campbell PA, Cohen JJ, Bratton DL, Henson PM. Exposure of phosphatidylserine on the surface of apoptotic lymphocytes triggers specific recognition and removal by macrophages. *J Immunol.* 1992;148(7):2207-2216.
45. Hochreiter-Hufford A, Ravichandran KS. Clearing the dead: apoptotic cell sensing, recognition, engulfment, and digestion. *Cold Spring Harbor perspectives in biology.* 2013;5(1):a008748.
46. Thum T, Bauersachs J, Poole-Wilson PA, Volk HD, Anker SD. The dying stem cell hypothesis: immune modulation as a novel mechanism for progenitor cell therapy in cardiac muscle. *J Am Coll Cardiol.* 2005;46(10):1799-1802.
47. Morelli AE, Larregina AT. Apoptotic cell-based therapies against transplant rejection: role of recipient's dendritic cells. *Apoptosis.* 2010;15(9):1083-1097.
48. Eisner C, Faulhaber-Walter R, Wang Y, et al. Major contribution of tubular secretion to creatinine clearance in mice. *Kidney international.* 2010;77(6):519-526.
49. Lazzeri E, Crescioli C, Ronconi E, et al. Regenerative potential of embryonic renal multipotent progenitors in acute renal failure. *Journal of the American Society of Nephrology : JASN.* 2007;18(12):3128-3138.
50. Pode-Shakked N, Pleniceanu O, Gershon R, et al. Dissecting Stages of Human Kidney Development and Tumorigenesis with Surface Markers Affords Simple Prospective Purification of Nephron Stem Cells. *Sci Rep.* 2016;6:23562.
51. Lindgren D, Bostrom AK, Nilsson K, et al. Isolation and characterization of progenitor-like cells from human renal proximal tubules. *The American journal of pathology.* 2011;178(2):828-837.
52. Schwartz JD, Dumler F, Hafron JM, et al. CD133 Staining Detects Acute Kidney Injury and Differentiates Clear Cell Papillary Renal Cell Carcinoma from Other Renal Tumors. *ISRN Biomarkers.* 2013;2013:8.
53. Sun Y, Yu H, Zheng D, et al. Sudan black B reduces autofluorescence in murine renal tissue. *Arch Pathol Lab Med.* 2011;135(10):1335-1342.
54. Sharkey J, Scarfe L, Santeramo I, et al. Imaging technologies for monitoring the safety, efficacy and mechanisms of action of cell-based regenerative medicine therapies in models of kidney disease. *European Journal of Pharmacology.* 2016;in press.
55. Toyohara T, Mae S, Sueta S, et al. Cell Therapy Using Human Induced Pluripotent Stem Cell-Derived Renal Progenitors Ameliorates Acute Kidney Injury in Mice. *Stem cells translational medicine.* 2015;4(9):980-992.
56. Bruce AT, Ilagan RM, Guthrie KI, et al. Selected renal cells modulate disease progression in rodent models of chronic kidney disease via NF-kappaB and TGF-beta1 pathways. *Regen Med.* 2015;10(7):815-839.
57. Woo DH, Kim SK, Lim HJ, et al. Direct and indirect contribution of human embryonic stem cell-derived hepatocyte-like cells to liver repair in mice. *Gastroenterology.* 2012;142(3):602-611.
58. Finan A, Richard S. Stimulating endogenous cardiac repair. *Front Cell Dev Biol.* 2015;3:57.
59. Eggenhofer E, Benseler V, Kroemer A, et al. Mesenchymal stem cells are short-lived and do not migrate beyond the lungs after intravenous infusion. *Front Immunol.* 2012;3:297.
60. Huen SC, Cantley LG. Macrophage-mediated injury and repair after ischemic kidney injury. *Pediatric nephrology.* 2015;30(2):199-209.
61. Deng J, Kohda Y, Chiao H, et al. Interleukin-10 inhibits ischemic and cisplatin-induced acute renal injury. *Kidney international.* 2001;60(6):2118-2128.
62. Luk F, de Witte SF, Korevaar SS, et al. Inactivated Mesenchymal Stem Cells Maintain Immunomodulatory Capacity. *Stem cells and development.* 2016;25(18):1342-1354.
63. De Jong OG, Van Balkom BW, Schiffelers RM, Bouten CV, Verhaar MC. Extracellular vesicles: potential roles in regenerative medicine. *Front Immunol.* 2014;5:608.
64. Gatti S, Bruno S, Deregibus MC, et al. Microvesicles derived from human adult mesenchymal stem cells protect against ischaemia-reperfusion-induced acute and chronic kidney injury.

Nephrology, dialysis, transplantation : official publication of the European Dialysis and Transplant Association - European Renal Association. 2011;26(5):1474-1483.
65. Shen B, Liu J, Zhang F, et al. CCR2 Positive Exosome Released by Mesenchymal Stem Cells Suppresses Macrophage Functions and Alleviates Ischemia/Reperfusion-Induced Renal Injury. *Stem Cells Int.* 2016;2016:1240301.
66. Collino F, Bruno S, Incarnato D, et al. AKI Recovery Induced by Mesenchymal Stromal Cell-Derived Extracellular Vesicles Carrying MicroRNAs. *Journal of the American Society of Nephrology : JASN.* 2015;26(10):2349-2360.

FIGURE LEGENDS

Figure 1. Identification and isolation of a population of human kidney cells. **(A)** Representative confocal fluorescence images of human kidney cells from infant human renal tissue showing the expression pattern of CD133 within the Bowman's capsule (highlighted by white arrows) and on the apical surface of scattered tubular cells. **(B)** Representative fluorescence images of bulk cultured cells at passage 1 after isolation, stained for CD133. Most of the cells appear CD133-positive. **(C)** FACS analysis showing the proportion of $CD133^+$ and $CD24^+$ cells within the bulk population at passage 2. The majority of the cells in the bulk population express CD133 (68.8% ± 9.2) and CD24 (86.10% ± 6.3). **(D)** Representative flow cytometry Dot Plot of the bulk population at passage 2 stained with CD133 (APC) and CD24 (FITC) antibodies. Magnification: (A-B) 400x, scale bar 50µm.

Figure 2. Both $CD133^+$ and $CD133^-$ human kidney cells can ameliorate renal function at day 7. **(A)** Experimental design. **(B)** FACS analysis of the expression of CD133 in both $CD133^+$ and $CD133^-$ populations at passage 5; mean values ± SEM of three independent sortings and expansions. **(C)** Mean FITC-sinistrin $t_{1/2}$ values ± SEM. **(D)** Serum creatinine levels. **(E)** Urea

levels. The dotted line represents the average of the respective baseline values of all animals (n=20). A one-way ANOVA statistical test with Dunnet *Post Hoc* analysis was applied to each data set for each time point to compare the groups. p-values are indicated in the tables below the graphs. $CD133^+$ group (n=6); $CD133^-$ group (n=6); cisplatin-injured group (n=7).

Figure 3. Both $CD133^+$ and $CD133^-$ human kidney cells ameliorate histological damage. **(A)** Representative images of H&E-stained kidney sections for each experimental group, including uninjured rats. The nephron tubules are noticeably damaged in the cisplatin-injured rats that did not receive cell therapy, but the glomeruli appear normal (see inset). Magnification 200x, scale bar 50µm. **(B)** The mean luminal area is significantly reduced in both cell-treated groups; $CD133^+$, p=0.0084; $CD133^-$, p=0.0147; one-way ANOVA statistical test with Dunnet *Post Hoc* analysis; error bars represent SEM. **(C)** Representative images of Masson's trichrome staining of kidney sections for each experimental group, including uninjured rats. Magnification 100x, scale bar 50µm. **(D)** Quantification of the fibrotic area in histological kidney sections after processing of at least 10 images per animal for each group; one-way ANOVA statistical test with Bonferroni *Post Hoc* analysis; error bars represent SEM. Abbreviations: pn, arrowhead – Pyknotic nuclei; fe, arrows – flat epithelium; d – dilated tubuli.

Figure 4. PKH26 dye but not GFP-positive cells are found in kidneys and lungs. Maximum intensity projection (MIP) confocal microscopy images of representative tissue sections of kidneys **(A-C)** and lungs **(D-F)**. In the kidneys, green autofluorescence is observed in all groups (white arrows). No GFP^+ cells could be detected in either the kidneys or the lungs. Punctate PKH26 label was found in both organs. Magnification: 400x, scale bars 100µm.

Figure 5. Human kidney cells are entrapped in the lungs and die within 24 hours. **(A-B)** Representative MIP confocal microscopy images of lung sections of animals at 1, 6 and 24 hours following cell administration. One hour after injection, some GFP^+ cells had apoptotic nuclei, indicated by the arrowheads **(A)**. **(B)** To confirm the identity of the GFP+ cells, immunostaining was performed with the human specific antibodies, HLA and Human Nuclei-HuNu. **(C-C')** By 6 hours after injection, a few intact GFP^+ cells were still present, and PKH26 was observed in neighbouring non-GFP host cells. **(D)** By 24 hours, PKH26 was found in a punctate pattern, near GFP-labelled cell fragments. **(E-H)** Representative confocal microscopy images showing the kidney cortex of animals sacrificed at 1 and 24 hours following cell administration, stained for HLA **(E-F)** or HuNu **(G-H)** and GFP. No GFP^+ cells were detected in the kidneys at any time point. Magnification: (A-D) 1000x, (E-H) 200x, scale bars 50 μm unless specified.

Figure 6. $CD68^+$ phagocytic cells cluster around the human kidney cells in the lungs. **(A-D)** Representative MIP confocal microscopy images showed CD68 signal (white) in lung sections from control and cell-administered animals at all time points. In sections from animals that received human kidney cells, $CD68^+$ cells were clustered around the GFP-labelled cells (white arrows). Scale bar is 100μm. **(B', D')** MIP confocal microscopy images at higher magnification, showing GFP (green), PKH26 (red) and CD68 (white). One hour after administration, $CD68^+$ cells were found clustered around the human cells in sections of lungs. **(D')** By 24 hours, some $CD68^+$ cells were localised around GFP^+ cell fragments (white arrow). Magnification: (A-D) 100x; (B'-D') 400x, scale bars 50 μm.

Table 1. Summary of the therapeutic efficacy observed in both cell-treated groups compared with the control groups. Percentage changes apply for FITC-sinistrin $t_{1/2}$, sCr and BUN at day 7, and for albumin:creatinine ratio, histological damage and fibrosis at day 14.

HUMAN KIDNEY-DERIVED CELLS AMELIORATE ACUTE KIDNEY INJURY WITHOUT ENGRAFTING INTO RENAL TISSUE

Running title: human kidney cells improve AKI without engrafting

Ilaria Santeramo[1]*, Zeneida Herrera Perez[2]*, Ana Illera[1], Arthur Taylor[1], Simon Kenny[3], Patricia Murray[1§], Bettina Wilm[1§], Norbert Gretz[2§]

SUPPLEMENTAL DATA

SUPPLEMENTAL METHODS

HUMAN CELLS AND TISSUE IMMUNOFLUORESCENCE

Upon reception, part of the human tissue was frozen for immunhistological analysis. 6 µm-thick sections were blocked with 0.1% Triton-X 100 (Sigma) and 10% Goat Serum (Sigma) in PBS and incubated with anti-CD133/1 (1: 50, Miltenyi) followed by secondary antibody Alexa Fluor® 488 nm goat anti-mouse IgG_1 (Thermo-Fisher Scientific). Fluorescence images were taken using a spinning disk confocal microscope CSU-X1 (3i), coupled with a digital camera (CMOS, Hamamatsu).

For the immunofluorescence experiments with cells, freshly isolated cells were plated in 8-well chamber slides (Corning), and grown until confluent. The cells were fixed in 4% PFA, blocked using 2% BSA (Sigma), 0.1% Triton-X in PBS and incubated with anti-CD133/2 (1:50, Miltenyi) followed by secondary antibody Alexa Fluor® 594-coupled goat anti-mouse IgG (H+L) (Thermo-Fisher Scientific). Fluorescence images were taken using an epifluorescence Leica DM2500 microscope coupled to a Leica DFC420C camera.

FLOW CYTOMETRY AND FACS

For the flow cytometry analysis of the $CD133^+$ and $CD133^-$ (shown in Figure 1C) cells, a BD FACS Calibur (BD Biosciences) was used. $5x10^5$ cells were labelled with CD133/1 APC (Miltenyi, 1:11), CD24 FITC (Miltenyi, 1:11), or both in 1% (v/v) FBS, 0.1% NaN_3 in PBS, according to the manufacturer instructions. Unlabelled cells were used to set the FSC, SSC and the fluorescence channels correctly. For FACS, a BD FACS Aria (BD Biosciences) was used. Cells were labelled with CD133/1 APC (1:11) in 1% (v/v) FBS at a concentration of 5-7.5x10^6 cells/ml. $5x10^5$ cells unlabelled or labelled cells were used to set the gates. Following the sorting, both populations were re-analysed to define the purity of the sorting and plated.

EXPANSION IN CULTURE OF $CD133^+$ AND $CD133^-$ CELLS AND FLOW CYTOMETRIC ANALYSIS

$CD133^+$ and $CD133^-$ cells were isolated using flow activated cell sorting (FACS) and expanded in culture. A low plating density was used for both cell types (2 x 10^5 per $10cm^2$ plate). The expression of CD133/1 APC was analysed by flow cytometry at each passage, using a BD FACS Calibur (BD Biosciences). In order to maintain a pure population of $CD133^-$ cells, magnetic activated cell sorting (MACS) was performing using CD133/1 PE (Miltenyi, 1:11) and Anti-PE Microbeads (Miltenyi, 40µl on LD columns). At passage 5 a sample of the $CD133^+$ and $CD133^-$ cells that were administered to the animals were analysed using flow cytometry. 0.5-1 x 10^6 cells were labelled with CD133/1 APC, CD133/2 PE, CD24 FITC, CD90 FITC, CD73 PE, CD105 FITC, CD44 FITC, CD326 FITC, CD324 APC (all from Miltenyi, 1:11) in 1% (v/v) FBS, 0.1% NaN_3 in PBS, according to the manufacturer's instructions. Unlabelled cells were used to set the gates for the forward scatter (FSC) and side scatter (SSC) and isotype specific control antibodies were used to set the gates for the fluorescence channels. For analysis of $CD133^+$ and $CD133^-$ cells, antibodies were used in combination with CD133/1 or CD133/2. Human MSCs were from Lonza and cultured according to the manufacturer's recommendations. 0.5-1 x 10^6 cells at passage 3 or 4 were labelled with CD133/1 APC, CD133/2 PE, CD24 FITC, CD90 FITC, CD73 PE, CD105

FITC, CD44 FITC, CD326 FITC, CD324 APC (all from Miltenyi, 1:11) in 1% (v/v) FBS, 0.1% NaN_3 in PBS, according to the manufacturer's instructions.

SUPPLEMENTAL FIGURES

Supplemental Figure 1. Sorting for GFP^+ $CD133^+$ and GFP^+ $CD133^-$ kidney cells. **(A)** Dot Plot showing FSC-A (Forward Scatter-Area) and SSC-A (Side Scatter-Area) used to discriminate healthy and damaged or dying cells in the bulk population. **(B)** Dot plot of SSC-A and FSC-W (Forward Scatter-Width) used to discriminate doublets, which might represent a false positive signal. **(C)** Density plot showing the signal from the excitation of cells with the 488-nm laser (GFP, FITC-A, log scale) against the signal from the FL4 laser (CD133, APC-A, log scale). A small percentage of $CD133^+$ cells was not efficiently transduced with GFP lentivirus ($CD133^+$ 4.9% vs $CD133^-$ 1.4%). **(D)** Percentage of CD133-expressing cells after sorting into $CD133^+$ and $CD133^-$ populations. **(E)** Representative images of transduced and un-transduced $CD133^+$ cells and $CD133^-$ cells at passage 3. The $CD133^+$ population mainly comprised epithelial cells, while the $CD133^-$ population contained mostly elongated mesenchymal-like cells. Magnification 100x, scale bars 100 μm.

Supplemental Figure 2. (A) Flow cytometric analysis performed on $CD133^+$ and $CD133^-$ cells from passage 2 (P2) to passage 6 (P6). In order to achieve a high purity of the $CD133^-$ population, CD133-specific MACS was used to purify the population at P3 and P4. The flow cytometric analysis of the cells at P5 (time-point of injection) is reported in **(B).** Characterization of the $CD133^+$, $CD133^-$ (P5, n=2) and human MSCs (hMSCs, P3-4, n=3) for mesenchymal and epithelial markers using flow cytometry. **(C)** Table indicating average ± SD of all the markers analysed in each cell type.

Supplemental Figure 3. Absence of GFP+ cells and evidence of tubular regeneration in the renal cortex 14 days after cell administration. **(A)** Representative stitched confocal images of

the renal cortex of animals belonging to the four experimental groups. Kidney sections were stained for megalin and GFP, and the confocal images stitched to a length of 2mm. In the cisplatin-injured group the pattern of megalin staining in some proximal tubules was atypical (arrows with triple heads), likely reflecting the fact that the PTCs in these tubules were injured. In contrast, the sections from cell-treated rats were indistinguishable from the uninjured animals. While no GFP signal was detected, unspecific green fluorescence was present, which was particularly strong in protein casts (*) and in cross-sections of tubuli (white arrows). **(B)** Representative confocal images of the renal cortex of animals stained for calbindin showed no differences between the different groups. **(C)** Albumin:creatinine ratio. The dotted line represents the average of the albumin:creatinine baseline values of all animals (n=20). An ANOVA one-way statistical test with Bonferroni's *Post Hoc* analysis was applied to each data set to compare the groups at day 14. $CD133^{+}$ group (n=7); $CD133^{-}$ group (n=6); control group (n=7). * p=0.0295; * p=0.0498 Magnification **(A)** 100x **(B)** 200x, scale bars 100 μm.

Supplemental Figure 4. Masson's trichrome staining shows negligible levels of fibrosis in cell-treated animals and injured controls. Representative stitched images of Masson's trichrome staining of kidney sections from animals of cisplatin-injured group, $CD133^{+}$-treated group, $CD133^{-}$-treated group and uninjured group. Magnification 100x, scale bar 100μm.

Supplemental Figure 5. Representative confocal MIP of the lungs of an animal sacrificed 1 hour after injection showing a GFP^{+} cell (left side) and an autofluorescent cell (right). Magnification 630x, scale bars 10 μm.

Supplemental Figure 6. Representative confocal images of the spleen of an uninjured rat (A), cisplatin-injured rat sacrificed 1 hour after injection of PBS (B), cisplatin-injured rat

sacrificed 1 hour after injection of $CD133^+$ cells (C), stained for GFP (green) and HuNu (white). Background autofluorescence was present in all samples but no signal was detected for human nuclei. Magnification 400x, scale bar 50μm.

Supplemental Figure 7. Representative confocal MIP of the lungs of animals sacrificed 1 **(B)** and 24 **(C)** hours after injection of $CD133^+$ cells stained for IL10 (red), CD68 (white), and GFP (green). At 24 hours, clusters of $CD68^+$ were observed, with an increase in the staining for IL10. White arrows identify green fragments belonging to GFP^+ cells. Magnification 400x, scale bar 50 μm.

SUPPLEMENTAL TABLES

Supplemental table 1. Mean values ± SEM for FITC-sinistrin $t_{1/2}$, serum creatinine, and urea for all groups at all time-points evaluated. An one-way ANOVA statistical test with Bonferroni *Post Hoc* analysis was applied to each data set to compare the values at baseline and at day 14. * $P<0.05$; ** $P<0.01$; *** $P<0.001$ one-way ANOVA with Bonferroni correction.

Supplemental table 2. Estimation of the extent of renal engraftment of $CD133^+$ cells reported in a previous study[a]

[a] See Ronconi et al., where 0.75 x 10^5 PKH26-labelled $CD133^+$ cells were injected into the tail vein of mice on the 1st and 4th day following the administration of adriamycin. On day 7, the total number of podocytes and proximal tubule cells (PTCs) were counted in histological sections by staining for podocin and LTL (Lotus tetragonolobus agglutinin). The proportion of $podocin^+$ and LTA^+ cells labelled with PKH26 was reported to be 11% and 7%, respectively. As indicated in the above table, the total number of podocytes and PTCs per mouse is estimated to be 3.6 x 10^5 and 12.8 x 10^6. Thus,

1. Nicholas SB, Basgen JM, Sinha S. Using stereologic techniques for podocyte counting in the mouse: shifting the paradigm. *Am J Nephrol.* 2011;33 Suppl 1:1-7.

2. Zhai XY, Birn H, Jensen KB, Thomsen JS, Andreasen A, Christensen EI. Digital three-dimensional reconstruction and ultrastructure of the mouse proximal tubule. *Journal of the American Society of Nephrology : JASN.* 2003;14(3):611-619.

3. Sakamoto H, Sado Y, Naito I, et al. Cellular and subcellular immunolocalization of ClC-5 channel in mouse kidney: colocalization with H+-ATPase. *Am J Physiol.* 1999;277(6 Pt 2):F957-965.

4. Murawski IJ, Maina RW, Gupta IR. The relationship between nephron number, kidney size and body weight in two inbred mouse strains. *Organogenesis.* 2010;6(3):189-194.

5. Ronconi E, Sagrinati C, Angelotti ML, et al. Regeneration of glomerular podocytes by human renal progenitors. *Journal of the American Society of Nephrology : JASN.* 2009;20(2):322-332.

11% of podocytes and 7% of PTCs would be equivalent to ~0.4 x 10^5 and ~0.9 x 10^6 cells, giving a total cell number of 0.94 x 10^6, which would amount to 63% of the injected cell dose (two administrations of 0.75x10^6 cells). Even if none of the cells died, which would be unlikely, and all passed through the lungs into the left ventricle, an engraftment level of 63% does not seem feasible because the kidneys only receive 20% of the cardiac output.

SUPPLEMENTAL VIDEOS

Supplemental video 1. Volume rendering of human CD133$^+$ cell in lung tissue 1 hour after cell injection.

Volume rendering of rat lung sections show a human GFP$^+$ CD133$^+$ cell (green) labelled with PKH26 (red), surrounded by CD68$^+$ cells (white). PKH26$^+$ can be observed in the proximity

of the human cell, co-localizing with $CD68^+$ cells. Imaris software was used to generate volume rendering, starting from a stack of confocal fluorescence images (section thickness 6 μm).

SUPPLEMENTAL VIDEO 2. VOLUME RENDERING OF HUMAN CD133+ CELL IN LUNG TISSUE 24 HOURS AFTER CELL INJECTION.

Volume rendering of rat lung sections show a fragment of a human GFP^+CD133^+ cell (green), surrounded by a cluster of $CD68^+$ cells (white). $PKH26^+$ (red) can be observed in the proximity of the human cell and within $CD68^+$ cells. Imaris software was used to generate the volume rendering, starting from a stack of confocal fluorescence images (section thickness 6 μm).

Figure 1

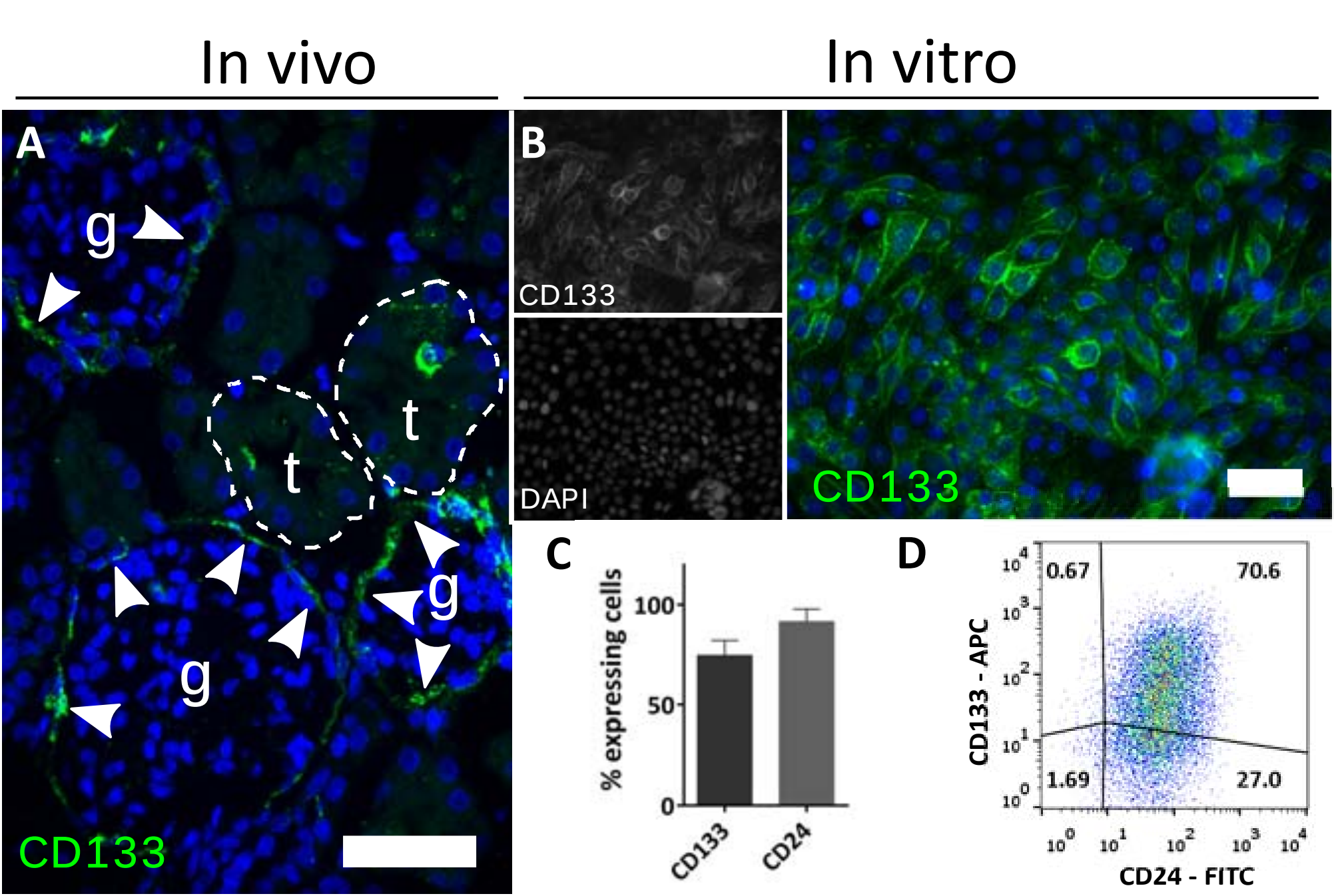
In vivo
In vitro
A
g
t
t
g
g
CD133
B
CD133
DAPI
CD133
C
% expressing cells
100
50
0
CD133
CD24
D
0.67
70.6
1.69
27.0
CD133 - APC
CD24 - FITC

Figure 2

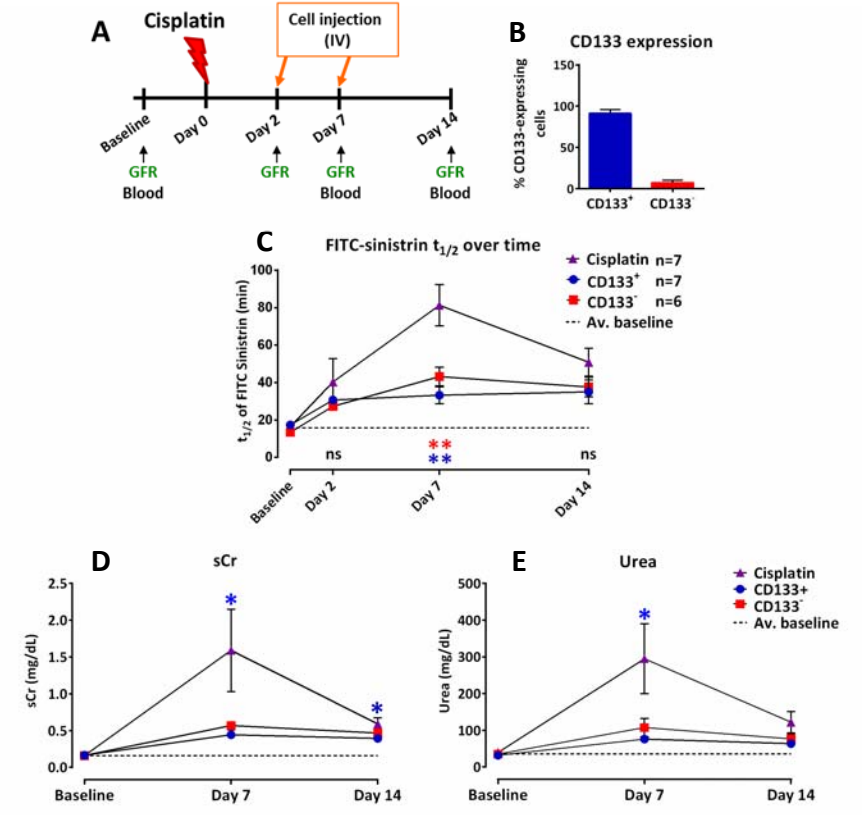

P-values (sCr)	Day 7	Day 14
Cisplatin vs CD133+	0.049	0.042
Cisplatin vs CD133-	0.095	0.25

P-values (Urea)	Day 7	Day 14
Cisplatin vs CD133+	0.03	0.087
Cisplatin vs CD133-	0.076	0.219

Figure 3

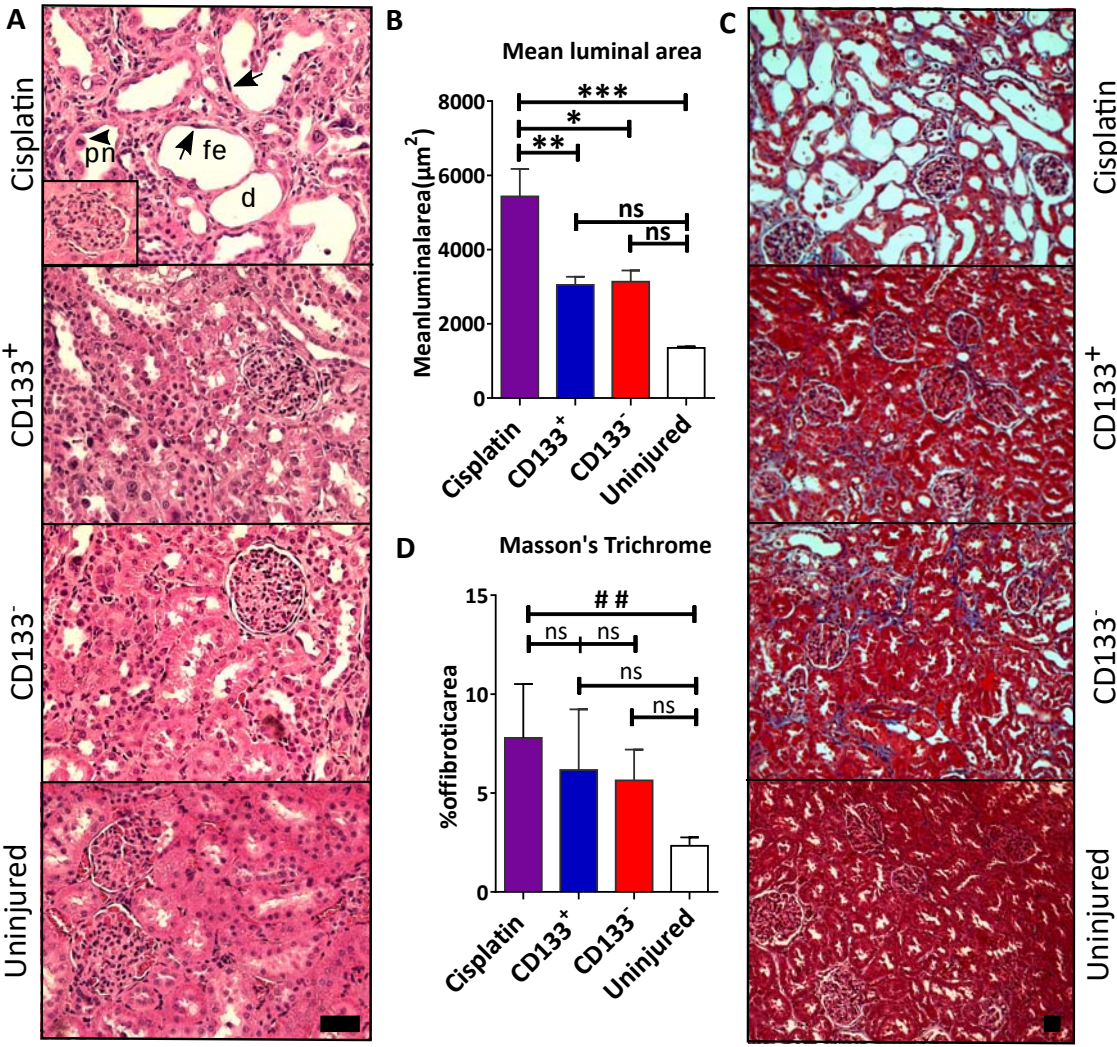
A
Cisplatin
CD133+
CD133-
Uninjured
pn
fe
d
B
Mean luminal area
Meanluminalarea(μm2)
8000
6000
4000
2000
0
***
*
**
ns
ns
Cisplatin
CD133+
CD133-
Uninjured
C
Cisplatin
CD133+
CD133-
Uninjured
D
Masson's Trichrome
%offibroticarea
15
10
5
0
# #
ns
ns
ns
ns
Cisplatin
CD133+
CD133-
Uninjured

Figure 4

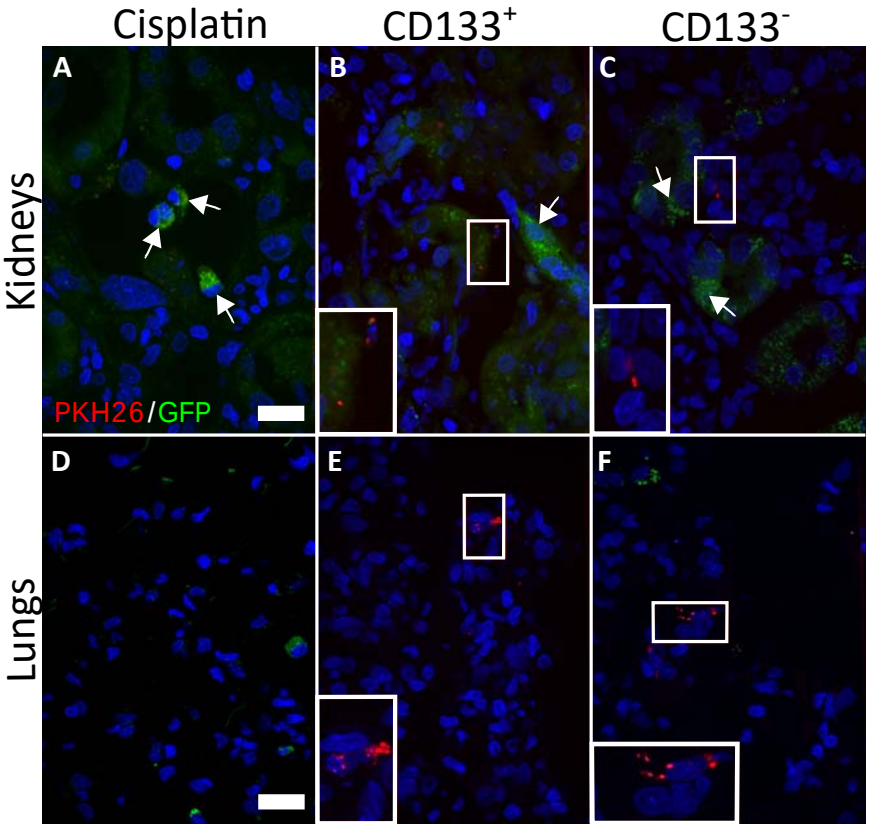

Figure 5

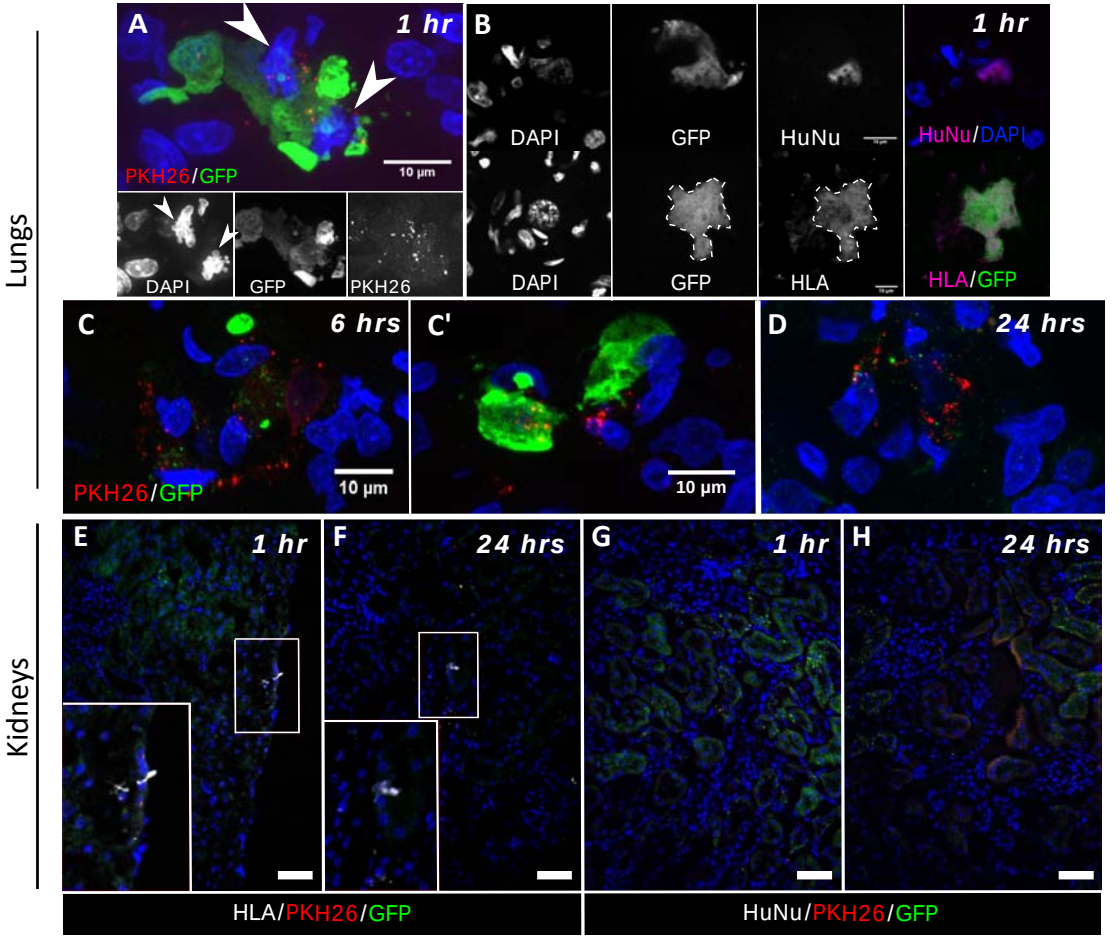
Lungs
Kidneys
A
1 hr
PKH26/GFP
10 µm
DAPI
GFP
PKH26
B
1 hr
DAPI
GFP
HuNu
HuNu/DAPI
DAPI
GFP
HLA
HLA/GFP
C
6 hrs
PKH26/GFP
10 µm
C'
10 µm
D
24 hrs
E
1 hr
F
24 hrs
G
1 hr
H
24 hrs
HLA/PKH26/GFP
HuNu/PKH26/GFP

Figure 6

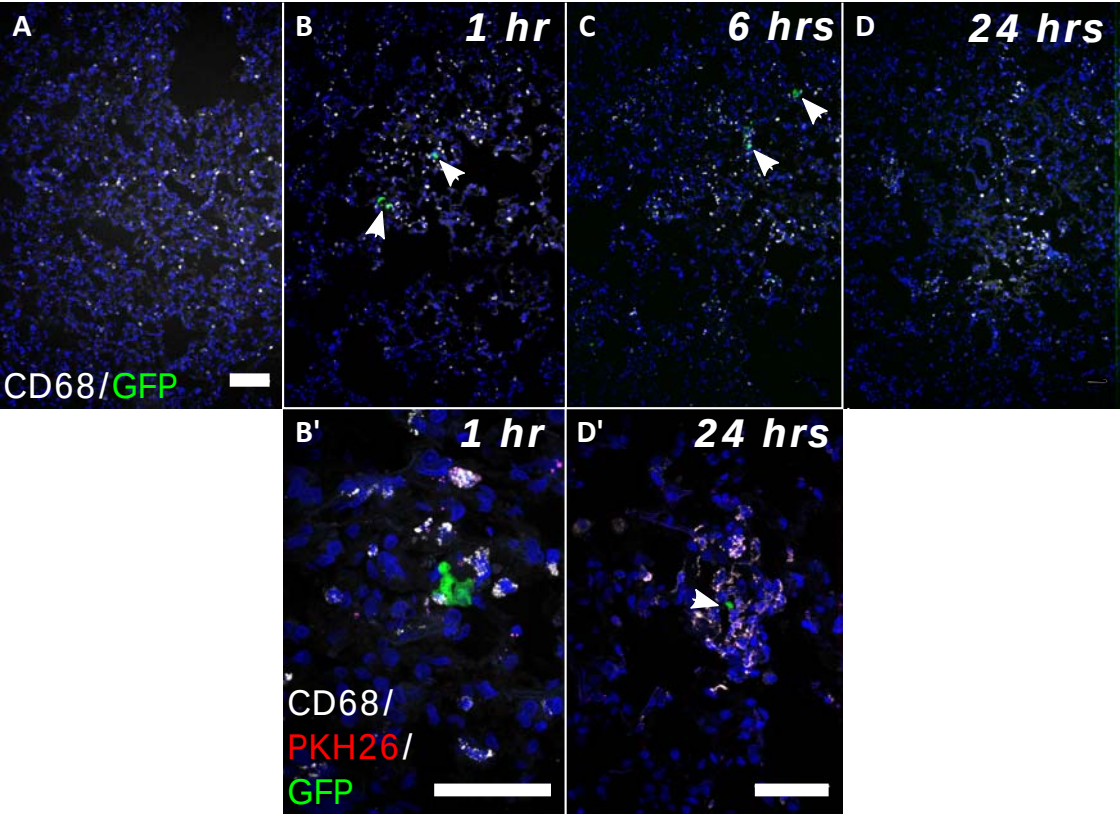

Supplemental Figure 1

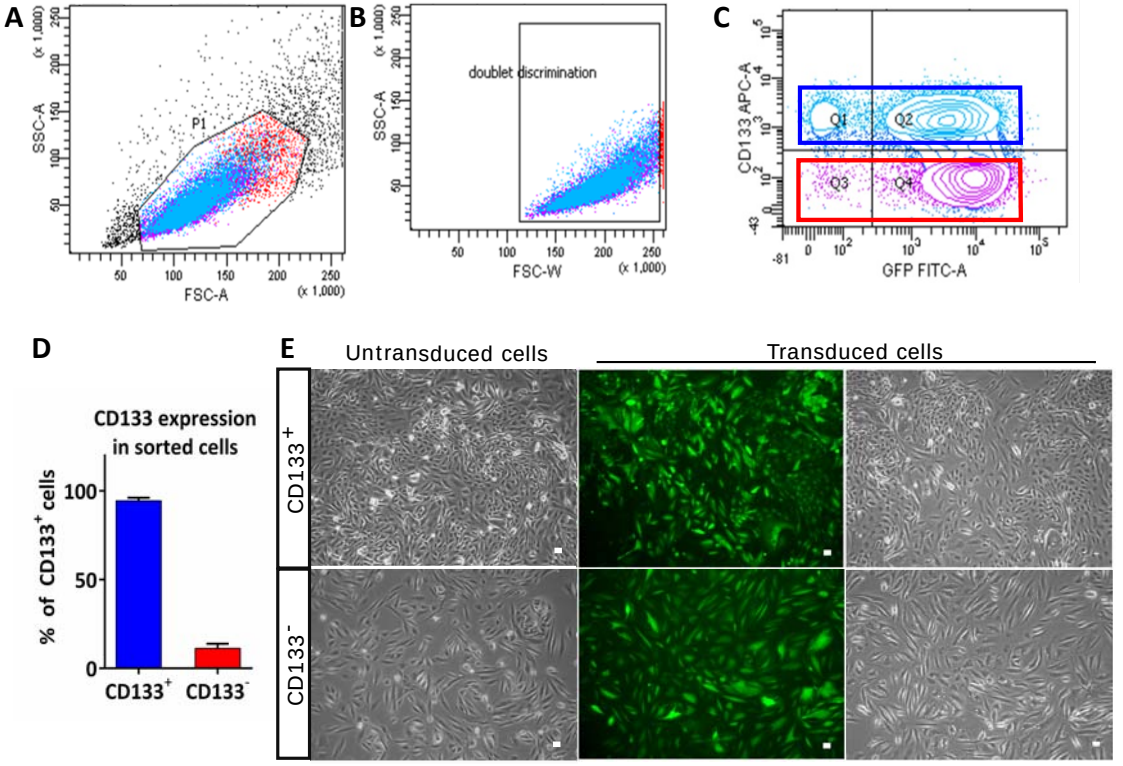

Supplemental Figure 2

A Expansion of CD133$^+$ and CD133$^-$ populations

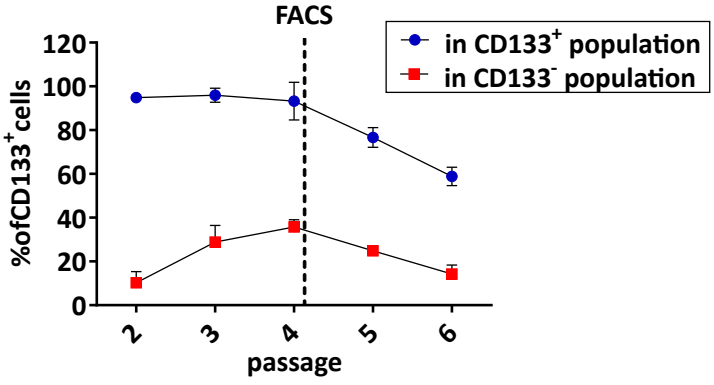

B

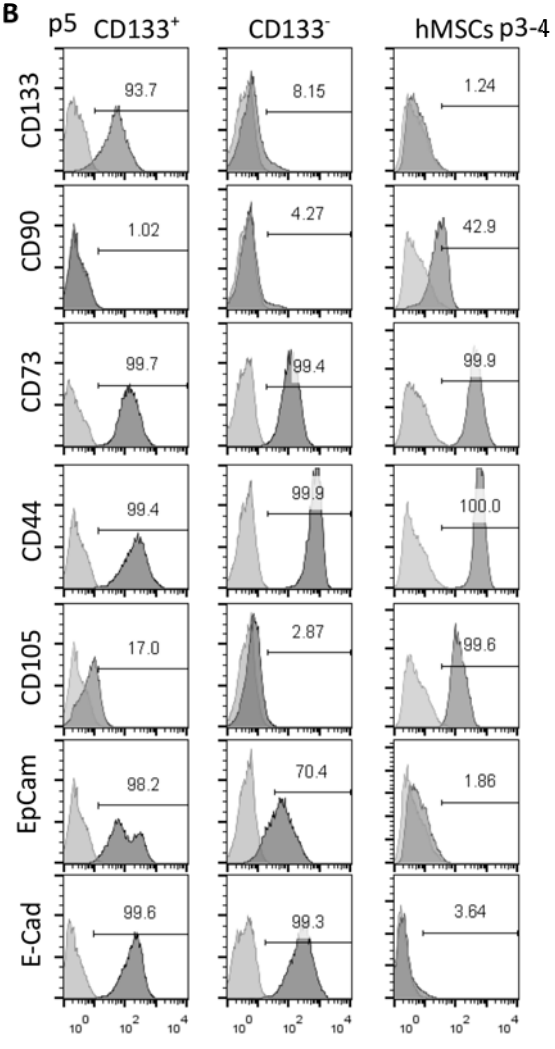

C

Marker	CD133$^+$	CD133$^-$	hMSCs
CD133	89 ± 6.65	11.63 ± 4.91	0.98 ± 0.19
CD90	1.175 ± 0.52	10.91 ± 9.46	14.41 ± 18.35
CD73	99.8 ± 0.14	99.35 ± 0.49	97.56 ± 2.71
CD44	99.65 ± 0.35	98.65 ± 1.63	98.73 ± 1.25
CD105	12.425 ± 6.61	1.97 ± 1.33	89.23 ± 9.3
CD326	98.85 ± 1.34	67.95 ± 3.46	1.24 ± 0.53
CD324	99.7 ± 0.14	99.3 ± 0.14	3.42 ± 1.63

Supplemental figure 3

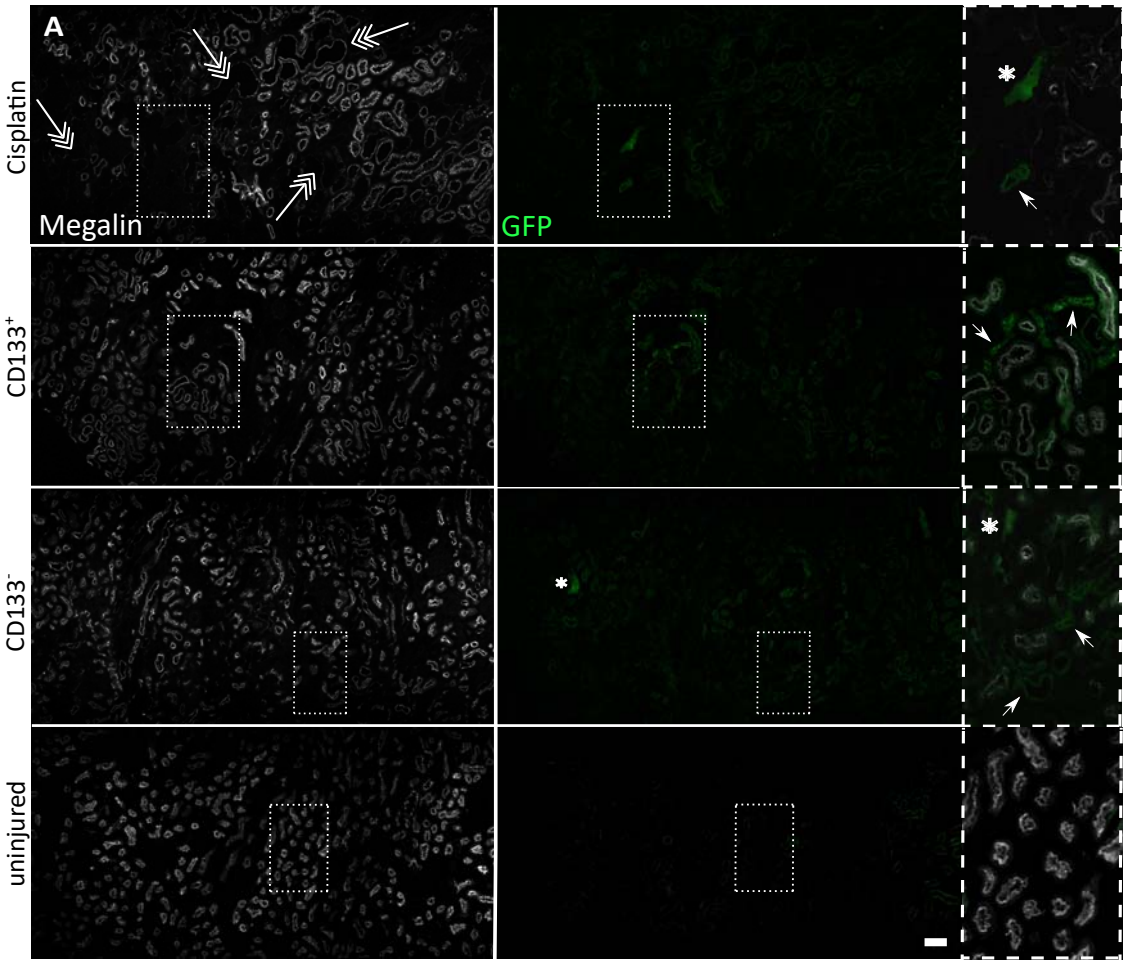

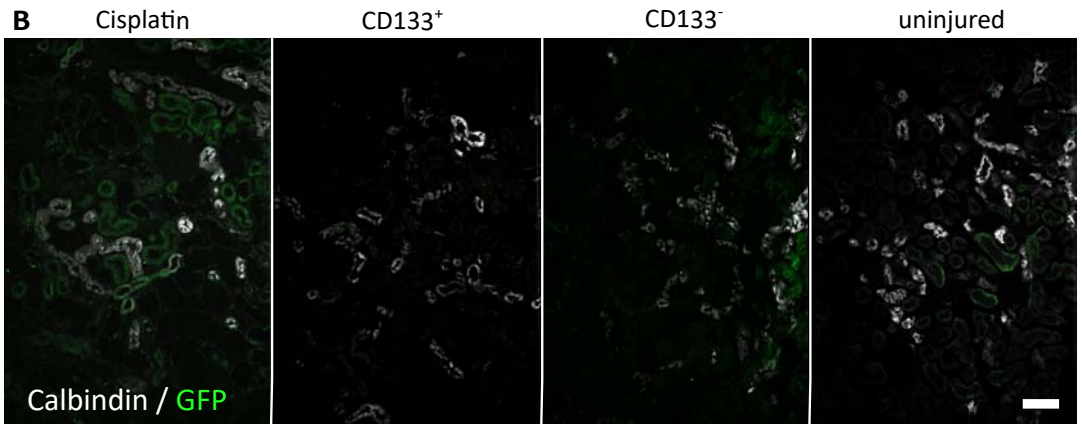

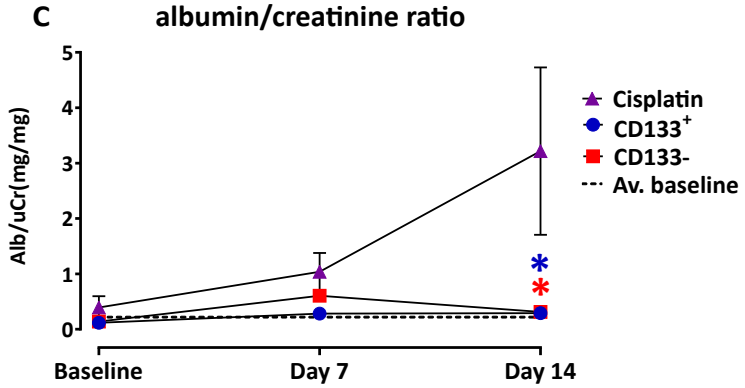

Supplemental Figure 4

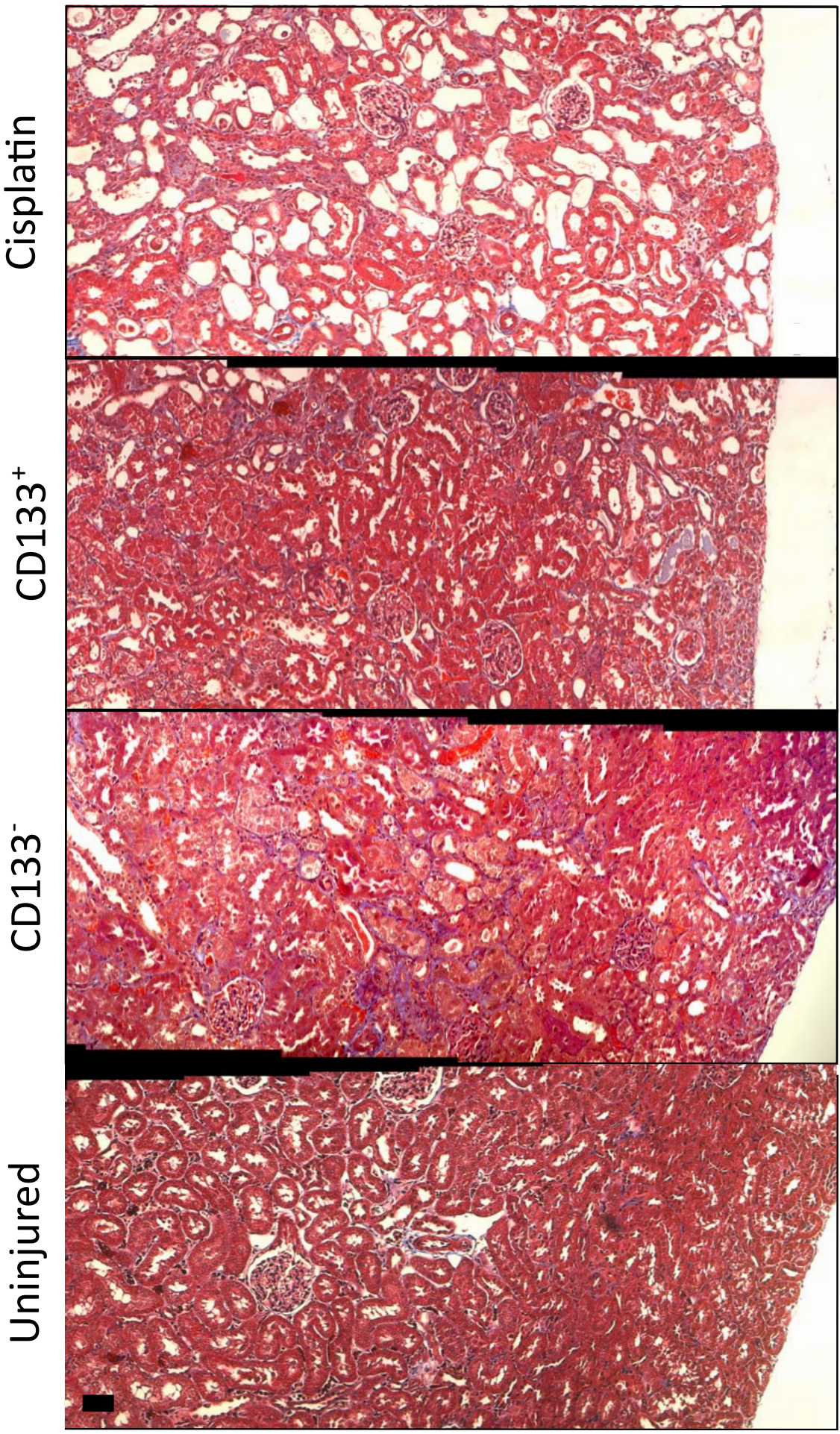

Supplemental Figure 5

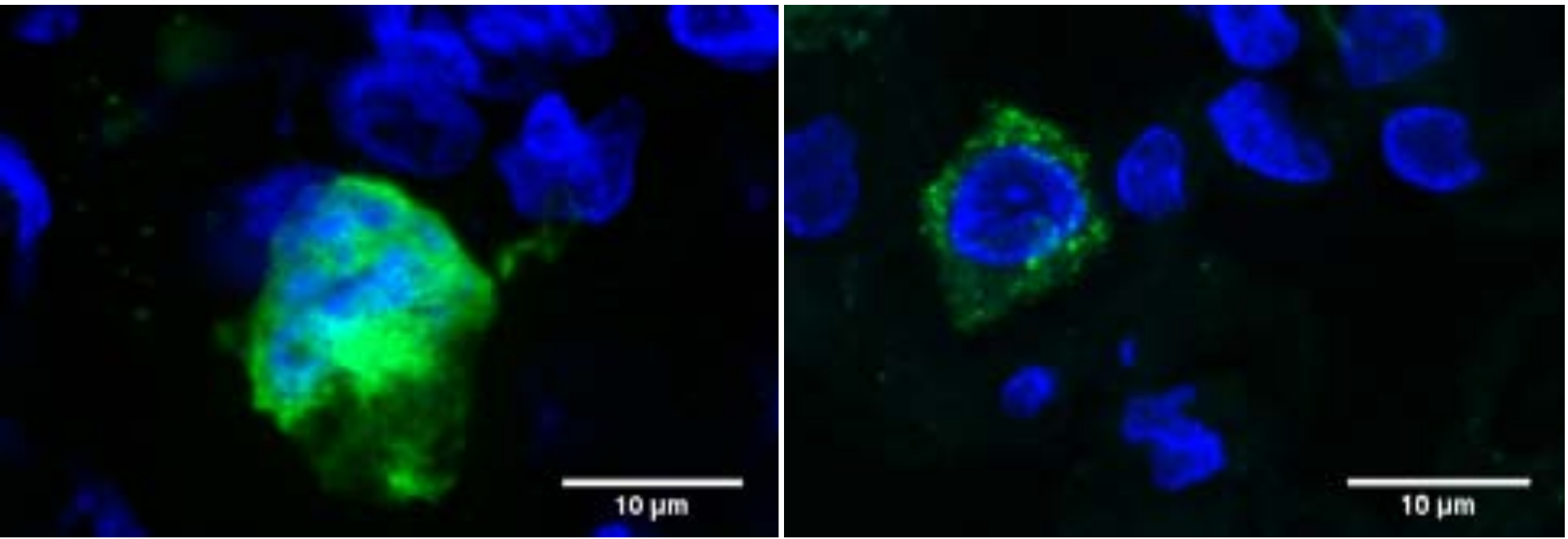

Supplemental Figure 6

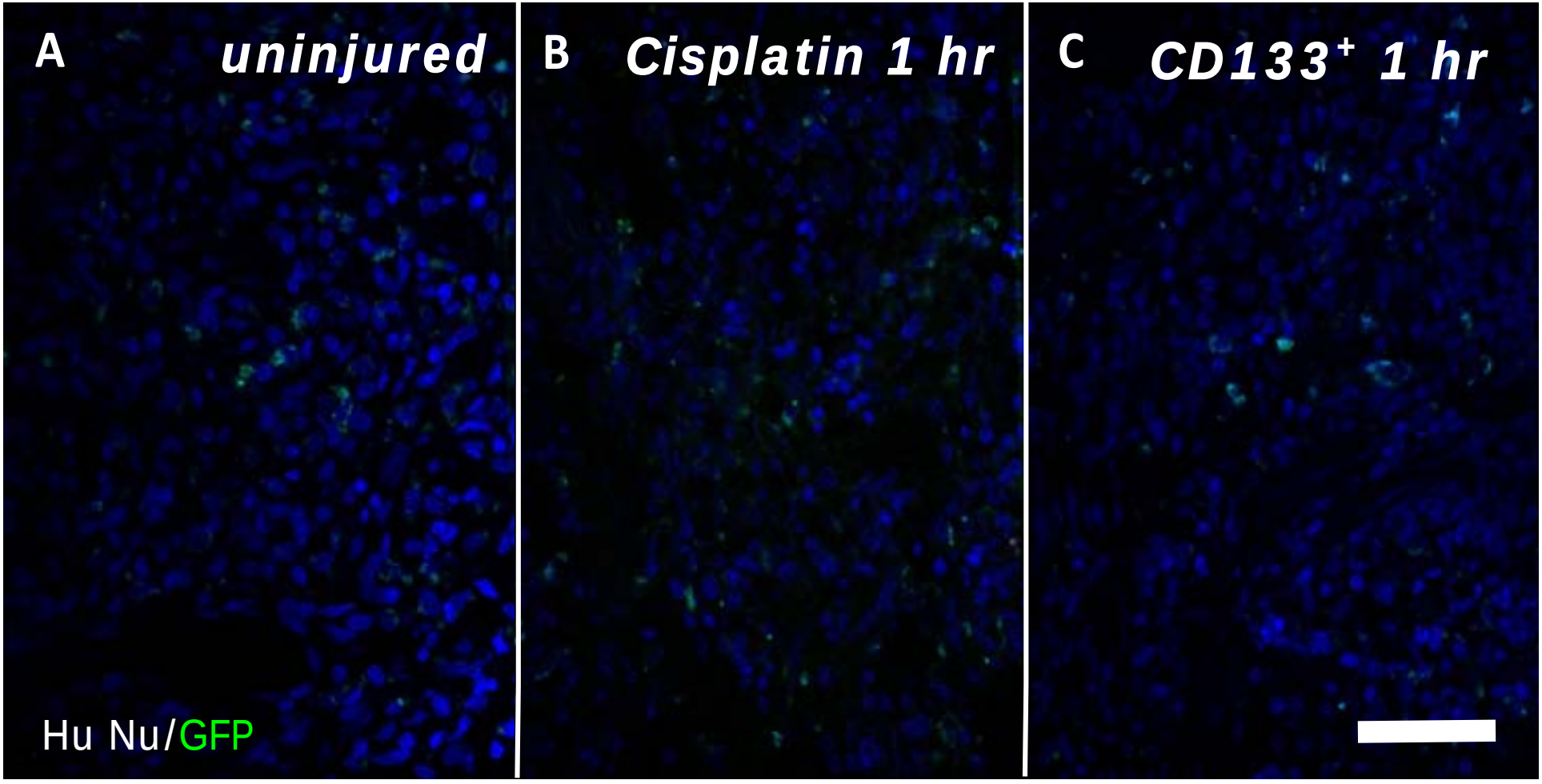

Supplemental Figure 7